Impacts of Warm and Cold situations in the Mediterranean Basins on the West African monsoon: observed connection patterns (1979-2006) and climate simulations

Bernard Fontaine, Javier García-Serrano, Pascal Roucou, Mb Rodriguez-Fonseca, S. Sijikumar, Sébastien Gervois, Fabrice Chauvin, Paolo Ruti, Serge Janicot

Impacts of Warm and Cold situations in the Mediterranean Basins on the West African monsoon: observed connection patterns (1979-2006) and climate simulations.

By Bernard Fontaine[1], Javier Garcia-Serrano[2], Pascal Roucou[1], Belen Rodriguez-Fonseca[2], Teresa Losada[2], Fabrice Chauvin[4], Sébastien Gervois[3], S. Sivarajan[1], Paolo Ruti[5] , Serge Janicot[3]

(1) Centre de Recherches de Climatologie, CNRS / University of Burgundy, Dijon, France

(2) Universidad Complutense de Madrid,Madrid, Spain

(3) Institut Pierre-Simon Laplace / LOCEAN, CNRS/IRD/Paris VI, Paris, France

(4) Centre National de Recherches Météorologiques, CNRS / Météo-France, Toulouse, France

(5) Environmental and Energy Research Institute, Roma, Italy

Abstract.

Using both empirical and numerical ensemble approaches this study focuses on the Mediterranean / West African relationship in northern summer. Statistical analyses utilize skin temperature, sea surface temperature, in situ and satellite rainfall, Outgoing Longwave Radiation (OLR) observations and reanalyzed data winds and specific humidity on isobaric surfaces. Numerical investigations are based on a large set of sensitivity experiments performed on four Atmospheric General Circulation Models (AGCM): ARPEGE-Climat3, ECHAM4, LMDZ4 and UCLA7.3. Model outputs are compared to observations, discussed model by model and with an ensemble (multi-model) approach.

As in previous studies the anomalous Mediterranean warm events are associated with specific impacts over the African monsoon region, i.e., a more intense monsoon, enhanced flux convergence and ascendances around the ITCZ, a strengthening of low level moisture advection and a more northward location of ascending motion in West Africa. The results show also new features (i) thermal variability observed in the two Mediterranean basins has unalike impacts, i.e. the western Mediterranean covaries with convection in Gulf of Guinea, while the eastern Mediterranean can be interpreted as Sahelian thermal-forcing; (ii) although observations show symmetry between warming and cooling, modelling evidences only support the eastern warming influence; (iii) anomalous East warm situations are associated with a more northward migration of the monsoon system accompanied by enhanced southwertely flow and weakened northeasterly climatological wind; (iv) the multi-model response shows that anomalous East warm surface temperatures generate an enhancement of

the overturning circulation in low and high levels, an increase in TEJ (Tropical Eeasterly Jet) and a decrease in AEJ (African Eeasterly Jet).

1. Introduction.

The potential role of surface temperatures over the Mediterranean in West African climate dynamics has been largely less investigated than that of the tropical Atlantic or of the El Nino Southern Oscillation (ENSO) phenomenon. Moreover these investigations are recent and hence only based on a few empirical and/or numerical studies. The seminal work, based on observed (1947–96) data, long-term Atmospheric General Circulation Model (AGCM) simulations and idealized experiments forced by warmer (colder) sea surface temperatures (SSTs) in the Mediterranean, has been published by Rowell in 2003. It demonstrates that "in years when the Mediterranean is warmer than average the Sahel tends to be wetter than normal" (and vice versa) with a significant positive correlation (r=+0.47) between the whole Mediterranean SST and JAS Sahel during 1947–96.

The same year Fontaine et al. (2003) used observational precipitation data and atmospheric reanalyses on the period 1968-1998 for studying moisture fluxes. They founded that part of the moisture fluxes vertically integrated in the layers 1000-300 hPa or 1000-925 hPa advected into the West African Monsoon area originates from the Mediterranean Sea and Central Africa and presents significant relationship with atmospheric water budget over the Sahelian belt during the rainy season. Contemporary, Raicich et al. (2003) found that the Sahel rainfall anticorrelates with sea-level pressure in the southeastern Mediterranean basin, suggesting the physical mechanism might involve variations in the local Inter Tropical Convergence Zone (ITCZ).

More recently, Peyrillé et al. (2007) analyzed the effect of changes in SST in the Mediterranean and the Gulf of Guinea using a 2-d zonally-symmetric model (30S to 40N), in modifying the thermal forcing (5°C warming from May to July). They showed that such a warming moistens the lower layers of the Sahara through advection and reduces the thermal gradient between the Saharan heat low and the Mediterranean, tending to decrease the NE winds (Harmattan). Finally using observations and reanalyses over multi decadal periods, Joly (2008) provided evidence of a significant intensification of the Mediterranean / West African relationship in last years.

However, up to date, there are some intriguing results regarding the thermal forcing of the Mediterranean Sea into the West African Monsoon (WAM) system. For instance, Rowell (2003) and Jung et al. (2006) described similar outcomes though using different SST patterns, prescribing thermal anomalies in the eastern and western Mediterranean basins respectively. There are also puzzling features concerning the atmospheric response related to Sahel precipitation, as local circulation anomalies (Raicich et al. 2003, Peyrillé et al. 2007) or 3-D

evidences for mechanisms favoring the northward migration of the monsoonal rainbelt (Peyrillé et al. 2007, Peyrillé and Lafore 2007). Indeed these empirical and numerical studies are either cases studies focusing on specific processes (i.e., Peyrillé et al., 2007), or analyzes taking into account the climatic transition which affected West Africa during the second par of the XXth century, i.e., the existence of a succession of anomalously wet years in the 50s and 60s followed by abnormally dry years in the 70s and 80s as in Rowell (2003). So the purpose of this study is not to reproduce and discuss previous results for resolving the questions above, but to reexamine the relationship through both historical data covering a period which does not include the negative tendency in West African precipitation between the 50s and 90s, and a lot of dedicated numerical GCM experiments.

This article focuses on the relationship between surface Mediterranean temperatures and the West African monsoon using Satellite observations and atmospheric reanalyses over the period 1979-2006 along with control and sensitivity experiments performed on 4 GCMs with an ensemble approach. The following section presents briefly the data used while section 3 portrays the basic features of the Mediterranean / African linear relationship through different SVD analyses of the temperature and Outgoing Longwave Radiation (OLR) fields and correlations with observed precipitation. Section 4 focuses on the observed contrasted impacts in Warm and Cold situations over the western and eastern Mediterranean basins to analyze both the linearity of the connection with the OLR signal and its impacts on observed atmospheric dynamics and Hadley circulation. In section 5, we will present different sensitivity experiments relative to the Mediterranean thermal variability performed on four climate models before analyzing the results in terms of rainfall impacts and atmospheric dynamics though an ensemble approach. Section 6 will propose a short discussion before the conclusion.

2. Selected historical datasets.

Land-based precipitation data (stations) do not allow accurate description of the West African rainfall variability at short time scales (i.e., lower than one month), especially in the recent years. This is mainly due to the anisotropy of the network, the number of stations documenting correctly rain falls being too low, especially along the meridional plane. For example the Global Surface Summary of Day dataset (GSOD) exhibits large areas without any station in the Benin, Togo and Burkina Faso positioned over the central parts of West Africa. Moreover some daily values are either not reported, or very underestimated or false

which changes the coverage with days, months and years. After the year 2000 the series are too incomplete for analysing accurately the daily or 5-day fields.

So for describing the monthly and seasonal time scales, we selected first the monthly precipitation from the high-resolution gridded CRU TS 2.1 data-set. These files comprise 1224 grids of observed climate, for the period 1901-2002, and cover the global land surface at 0.5 degree resolution (see *New et al, 2002 and Mitchell et al, 2004*). For shorter time scales, rainfall information has been selected from the CPC Merged Analysis of Precipitation [CMAP, *Xie and Arkin*, 1997] and from the Global Precipitation Climatology Project [GPCP, *Adler et al*, 2003 and *Xie et al*, 2003] estimates on a 2.5 x 2.5 degree latitude/longitude grid at a 5-day time-scale over the period 1979-2006. These satellite-derived estimates do not describe exactly the real world but have many advantages over current in situ data: they are coherent in space and time at 5-day scale, they have been often described and used and they give access to different information. However in northern summer, the mean precipitation differences (CMAP –GPCP) are positive over land and negative over Ocean with a typical difference of ± 0.1 mm/day (*Gruber et al*., 2000). This could be due to the fact that, by contrast with GPCP, CMAP uses uncorrected rain gauge over land (*Gruber et al.*, 2000). Moreover, Yin et al. (2004) indicate that (i) the GPCP/CMAP spatial correlation is higher over land than over ocean; (ii) in general precipitation over ocean represented by the GPCP is more accurate while over land the two products are close. More details can be found in Louvet et al. (2007).

The Sea Surface Temperatures provide from the most current version of the Kaplan dataset produced by taking the MOHSST5 version of the GOSTA data set from the U.K. MET office and using EOF projection, optimal interpolation, Kalman Filter analysis, and an optimal smoother for filling in any missing data. The data set is stored on a 5x5 grid.

Skin temperatures and atmospheric data in all the troposphere provide from National Centers for Environmental Prediction (NCEP) and is called NCEP/DOE AMIP-II Reanalysis (R-2) over the period 1979-2006. This dataset can be hence considered as a mix of in-situ and satellite observations and modelling. It improves however upon the NCEP/NCAR Reanalysis (R-1) by fixing the errors and by updating the parameterizations of the physical processes. It has been also extensively used and described (Kanamitsu et al., 2002; Maurer et al., 2001 among others). To be very concise one can say that R-2 provides more accurate pictures of soil wetness, near surface temperature and surface hydrology budget over land, and radiation fluxes over Ocean. The new boundary layer and convection schemes have also modified the water vapor profile: R-2 has more moisture in low levels than R-1.

The daily NOAA Interpolated Outgoing Longwave Radiation (OLR) data are used in a 2.5°*2.5° version where all gaps have been filled with temporal and spatial interpolation as described in Liebmann and Smith (1996). OLR is an interesting additional dataset for our purpose since it measures the direct emission from the surfaces (Earth, clouds). It allows therefore clear depiction between clear-sky regions which concentrate the highest OLR values from the warmest surfaces and deep convective regions where the highest and coldest clouds (cirrus and tops of cumulonimbus) dominate. However OLR values in W/m2 are not direct measurements of deep convection since for example in clear-sky situations, OLR measures the direct emission from the warmer land or oceanic surfaces.

3. Basic features of the Mediterranean / African relationship

The relationship is here examined through several spatial indices and objective field analyses using SSTs, skin temperatures, precipitation and OLR.

3.1. Composite and correlation analyses through observed precipitation

This section illustrates the basic relationship observed at monthly scale using selected spatial indices describing North African rainfall and the Western and Eastern Mediterranean surface temperatures over the recent period 1979-2002. Table 1 presents first the rainfall means in mm observed in North Africa (5°N-20°N) and in the Sahelian belt (13°N-18°N) for both the boreal summer (JAS) and the months from May to October. The Warm minus Cold (W-C) differences (see the legend of table 1 for more details) are displayed in lines 3 and 4. Two important points emerge: (i) in boreal summer the warmest situations in the Mediterranean are associated with rainfall excess over North Africa and the Sahel and are preceded by rainfall deficits in spring; (ii) this relationship seems to reinforce when the Eastern Mediterranean and the Sahel band are considered although only the North African index in September can be considered as significantly different.

Table 2 allows us give more details regarding the relative weight of long-term (> 8 years) and inter-annual (< 8 years) variability in different July-September spatial indexes describing skin temperatures over the West and East Mediterranean, and the GPCP and CMAP rainfall estimates averaged over central Sudan (9°N-13°N) and the western (17°W-10°W), central (10°W-10°E) and eastern (10°E-20°E) Sahel (13°N-18°N) . Several important points can be mentioned. First the strongest significant correlations are generally registered with the GPCP estimates. Second the relationship between Sahelian rainfall and the Mediterranean thermal variability is significantly stronger when thermal variances < 8yr are

considered, above all in CMAP estimates. Thirdly the mean correlation between skin temperatures in the 2 basins and the Sudan-Sahel rainfall equals +0.31 (9% of variance, not significant taking into account autocorrelation in the series) with unfiltered series but increases to +0.49 (24% significant at p= 0.05) when variability lower than 8 yr is taken into consideration. Although the difference between these values is not very large, this is rather different from Rowell (2003) who, given the period analyzed (1946-1996), took mainly into consideration the long-term negative trend in West African rainfall: r=+0.61 for variability > 8 yr and +0.31 for < 8 yr. Notice also that thermal variability in the Eastern Mediterranean explains in mean 20% of the Sudan-Sahel rainfall total variance while the Western basin explains only 7%.

3.2. Robustness of the relationship

The linear relationship is further analysed by computing several Singular Value decompositions (SVD) between temperature fields and OLR fields over the period 1979-2005. Interpolated OLR data are a practical estimate of convective activity over West Africa, since OLR values < 240 W/m2 depict the occurrence of high clouds closely linked to deep moist convective areas as those which are positioned within ITCZ. These SVDs have been performed both at monthly, 5-day and daily scales in isolation to be not confounded with longer-term variations and using different time filters. The main results are reported in Figures 1 and 2 and Table 3.

Figure 1 refers to a synchronous (no lag) analysis performed between monthly skin temperatures observed over an extended Mediterranean region (5W-40E; 20N-45N) and monthly OLR values referring to an extended WAM region (20W-40E; 10S-20N). The total covariance equals 32.7% of the total variance and the squared covariance fractions of the two leading modes match 33.4% and 22.5% respectively. The first heterogeneous mode and its related time coefficients are displayed in Figure 1a,b. They clearly attest the statistical linkage between warm anomalies restricted to Eastern Mediterranean and low OLR anomalies expanding along 10N-15N and eastward to about 10W. As noticed above, the Eastern Mediterranean concentrates the highest positive loadings, while the western basin and continental regions somewhat northward to the mean ITCZ position accumulates the strongest negative loadings (meaning enhanced deep convection) with the maximum located in the central and eastern Sahel. Such a result agrees well with those shown by Polo et al. (2008) at monthly-interannual scale, suggesting an active role of the eastern Mediterranean SST into the

Sahelian variability. In fact, the coupled OLR and temperature time series in Fig. 1b are largely correlated (r=+0.70, significant at p=0.01 taking into account autocorrelation in the series); they display both an in-phase interannual signal and the recent rainfall recovering since the 90s. When these coefficients are averaged over the successive JAS season its correlation increases to +0.87, while the temperature and OLR time series are positively correlated with JAS rainfall averaged over central (10W-10E) Sahel: +0.50 and +0.67, significant at p=0.05 and p=0.01 respectively, taking into account autocorrelation in the series.

By construction the second skin temperature-OLR mode (Fig. 1c,d) is less energetic and registers lower serial correlation between time series (r=+0.61, significant at p=0.01 taking into account autocorrelation in the series). However it is the direct complement of the first one: the strongest (positive) temperature loadings are here restricted to the West Mediterranean. A surface warming in this region is linked to lower OLR values (deeper convection) extending both in the Western parts of the Sahel (Senegal, Mali) and over equatorial eastern Atlantic (Gulf of Guinea). When time coefficients are averaged over the JAS seasons the correlation increase to +0.70 (p=0.01), and the temperature and OLR time series are positively correlated with JAS rainfall over the western parts (18W-10W) of the Sahel: +0.31 and +0.43 respectively, this last value being significant at p=0.05.

In fact the Mediterranean/WAM relationship is not purely synchronous as illustrated in figure 1c. This diagram displays the lead/lag correlation coefficients computed between spatial indexes averaging OLR values in the Sahel zone (10°N-20°N; 15°W-30°E) in JAS, at the heart of the rainy season and 3-month surface temperatures in the whole Mediterranean basin (32°N-40°N; 6°W-36°W) moving with a 5-day (pentad) time-step before and after JAS. Near all the values are significant at p=0.05 but the strongest correlation is registered when the Mediterranean temperatures are leading OLR by 6 pentads (one month).

3.3. Evolution of the leading skin temperature / OLR mode at the monthly scale

In order to assess better the robustness of the Mediterranean / WAM lagged relationship, Figure 2 refers to SVD analyses performed at the monthly scale between Mediterranean skin temperatures and WAM OLR values one month later referring to the same domain that in Fig.1. Here linear trends in the series have been removed and the display focuses on the May/June to October/November evolution of the lagged temperature/OLR relationship. The results confirm first the statistical linkage between the East Mediterranean and WAM domains shown above (Fig. 1a). Second they show that there is no negative OLR

anomaly over the Sahel before Jun/July (Fig. 2b), confirming the previous dry regime as indicated from Table 1 (in May/Jun; Fig. 2a). There, warm anomalies are associated with positive values of OLR over Sudan-Sahel, meaning decreased convection. From Jul/Aug to Oct/Nov temperature loadings reinforce on the eastern Mediterranean according to the leading monthly coupled mode (Fig. 1a), while OLR anomalies are related to increased deep motions (Figs. 2c-f).

Once again, the East Mediterranean concentrates the highest positive temperature loadings in connection with WAM deep convection, which points out largest anomalies along 10N-15N and mainly located over inland regions. Also at daily scales, Table 3 summarizes the percentages explained by each leading JAS-mode, time correlation between time series before and after removing all linear trends at each grid point (columns 1-2). In fact the field coupling is slightly lower when the series are detrended with a leading mode, spatially similar to figure 2a but less energetic (29% vs 52% of squared covariance fraction) and positively correlated (+0.42 vs +0.51). Other columns underline possible connections with oscillatory modes at synoptic scale (< 10 days) such as African Easterly Waves (AEW) in the 3-5 day range, when longer-term mean coefficients are removed.

To test the linearity of the connection the next section contrasts the signals observed in warm and cold situations over the Western and Eastern Mediterranean.

4. Contrasted impacts in Warm and Cold situations

4.1. OLR signal

The mean July-September OLR field displayed in figure 3a exhibits high OLR values in the Mediterranean region and low OLR values near the ITCZ mean location since in dry subtropics (no cloud), OLR depends mainly on surface temperatures and is generally greater than 260 W/m2: any surface warming (cooling) in the lowest levels of the troposphere over the Mediterranean tends to enhance (reduce) OLR values. By contrast, in the vicinity of the ITCZ which concentrates the lowest OLR values (< 240 W/m2 in Fig. 3a) OLR is directly linked to the altitude of clouds (convective towers).

The warm (cold) composites relative to the Western and Eastern Mediterranean are shown in Fig. 3b and 3c, respectively (Fig. 3d and 3e). They contrast the 8 warmest and the 8 coldest seasons versus all the remainders (caption in Fig. 3 indicates the selected years). Once again the signal is more significant in figures 3c and 3e, i.e. when the possible thermal forcing involves the East Mediterranean: warm (cold) anomalies in the Eastern basin are associated

with lower (higher) OLR values. This denotes an enhancement (a reduction) of deep convection in the monsoon region when the East basin is abnormally warm (cold) and suggests hence the existence of associated signals in atmospheric dynamics.

4.2 . Atmospheric dynamics

Vertical cross sections of wind and specific humidity along the 20W-0° and 0°-30°E meridional planes and relative to the West and East Mediterranean are presented in figure 4. Panels a,b show the mean location and intensity of cell circulations along with the regions where specific humidity exceeds 10g/Kg. The northern and southern overturning cells are easily recognizable between the humid Mediterranean and monsoon regions (shading). The southern cell, where the monsoon takes place, includes southerly/northerly horizontal branches in low/high levels and ascending/ subsiding branches located respectively by 8-10°N and 20°S. Westward to the 0° meridian the strong ascents are associated with strong northerlies at 200 hPa southward to the equator (Fig 4a) which tends to fuel monsoon overturning in the southern cell. By contrast eastward to the 0° meridian the ascents fuel preferentially the northerlies in low levels from the Eastern basin and hence the northern cell (Fig. 4b).

Warm composites in figures 4c-f exhibit significant signals in both meridional circulation and specific humidity especially. Warm conditions in the Western basin are associated, westward to 0º, with lower-levels convergence and upper-levels ascending motions in the northern subtropical latitudes, and with significant moisture increase (shadings in Fig. 4c) in the low and mid troposphere above the equatorial Atlantic. However only 3% of the area can be considered as significant and there is no clear meridional-connection between the former and the latter. Neither a clear signal appears eastward to 0º. By contrast warm conditions in the Eastern basin reinforce the southern (monsoon) cell circulation between 0° and 30°E (fig. 4f) with 5 % of global field significance): low level advections from the South in temperature and moisture are significantly enhanced, while air ascents within the ITCZ and air descents above the Southern Tropics strengthen. This is accompanied by a significant moisture increase (shading in figure 4f) under 400 hPa over the continent (5°N-20°N). To a lesser extent, but of equal statistical significance, the northern Hadley cell is also reinforced showing a closed circulation.

The results reported in sections 3 and 4 are thus compatible with the existence of a significant statistical relationship between the East Mediterranean and the WAM-Sahel region. In order to check whether this is interpretable in terms of Mediterranean forcing, we

will analyze multi-model outputs using SST sensitivity experiments performed on 4 AGCMs. This approach allows production of more reliable climate features than a single model method since climate simulations performed on any given model are sensitive to systematic errors, as previously shown by, among others, Bader and Latif (2003) and Giannini et al. (2003).

5. Numerical study

5.1. Description of the sensitivity experiments

Several SST sensitivity experiments linked to normal, warm and cold situations over the Mediterranean have been performed on four AGCMs:

- ARPEGE-Climat Version 3 IPCC-AR4 in truncature 42 with 45 levels run at CNRM (Centre National de Recherches Météorologiques, Météo-France)
- ECHAM Version 4 in truncature 30 with 32 levels run at ENEA (Italian National Agency for New Technologies, Energy and Environment)
- LMDZ Version 4 (96 long, 71 lat and 19 levels) run at IPSL (Institut Paul-Simon Laplace)
- UCLA Version 7.3 (2° long * 2.5°lat, 29 levels) run at UCM (Universidad Complutense de Madrid).

In these experiments the SST anomaly patterns were calculated from observed ERSST dataset (Smith and Reynolds 2004) and over the period 1979-2005. The African Monsoon Multidisciplinary Analyses (AMMA) community decided that the boundary conditions were based on the expansion coefficient of the leading Extended Maximum Covariance mode between WAM-precipitation (CMAP dataset) and Mediterranean-SST described in Polo et al. (2008). This mode show strong positive links between the Sahelian rainfall and the spring to summer evolution of the SST anomalies in the eastern Mediterranean. In order to introduce some physical considerations in the SST patterns definitions, a SST composite was constructed by averaging years for which the phasing between SST and African precipitation was maximal. They have been computed chosen those years in which the SST and June-September precipitation expansion coefficients were higher than 1 standard deviation (1984,1987,1991,1992,1997) and those in which the expansion coefficients were less that -1 standard deviation (1979,1994,1999,2001). In order to amplify the SST signals, it has chosen to compute the difference between the positive-composite and the negative-composite of SST anomalies for defining the positive phase of the thermal forcing; while the negative phase was computed by multiplying the positive phase by -1. The SST anomalous patterns were finally multiplied by two in order to amplify the atmospheric response (Fig. 5). SST conditions have then been prescribed with these anomaly patterns added to the climatology of observed global SST for the period 1979-2005.

The ENEA, IPSL and UCM institutions performed 10 simulations with different initial conditions for each experiment (cold, warm, and control with no superimposed SST anomaly) while CNRM performed 20 simulations, allowing available a total of 150 simulations. However to give each model the same weight, we will consider 10 simulations for each model and each experiment (control, cold and warm), hence 10x4x3=120 simulations. Experiments have been run from 15th of April to 15th of October and each SST pattern have led to a set of 10 runs (20 runs for CNRM). Initial conditions have been taken from a long-term AMIP-type run with conditions representative of the end of the 20th century. A good way to do this was to take conditions around the 15th of April for 10 (or 20 for CNRM) different years in the set of possible initial conditions. The 10 (or 20) years for initial conditions have been taken from years 1979 to 1988 (or 1979-1998 for CNRM).

It is noteworthy that using such prescribed SST as a lower boundary condition implies that the sea acts as a reservoir of infinite heat capacity which is not the case in the real world where the Mediterranean has finite heat capacity. This tends to damp the surface heat fluxes and therefore to decrease the amplitude resulting from the model runs.

5.2 Multi-model rainfall outputs

In order to validate models outputs, figure 6 shows the May to September mean monthly rainfall fields averaged over the period 1979-2001 in the CPC merged precipitation and in the control experiments of each model. Nearly all models reproduce well seasonal evolution of the rainbelt both in terms of meridional displacements and of location of rainfall maxima (amounts > 6 mm/d are shaded). However systematic biases exist in each model. For example, the CNRM, IPSL and ENEA simulations tend to underestimate the rainfall amounts while UCLA overestimates. Notice also that the seasonal excursion of the rainbelt in latitude is better reproduced in CNRM and UCLA outputs (see also the Hovmoller diagrams for the control runs in Losada et al. 2009; this issue).

The 40 warm (W) and 40 cold (C) experiments limited to the Mediterranean are now compared to the 40 control simulations (CTL=climatology) regarding rainfall outputs from each model. The focus is made on the two main West African rainy seasons, i.e., the first Guinean rainy season in May-June (MJ) and the northern tropical rainy season in July-September (JAS).

Figure 7 displays the W-CTL and C-CTL field differences with superimposed shadings where they are significant. In MJ there is no coherent signal: i.e., the IPSL model produces significant rainfall differences (Fig. 7i,j, with 11% and 5% significant grid points, respectively), but with the same sign in both experiments. In JAS the responses are larger and increase in magnitude and significance. Even so, cold experiments generate fairly unclear results and are not conclusive at all, except with UCLA in Fig. 7o (6%). In contrast, warm experiments produce significant Sahelian rainfall excesses in 3 out 4 models (CNRM, IPSL, UCLA with respectively 10%, 18% and 9% significant points), which outputs are in good agreement with our previous empirical results. The precipitation response from ENEA does not yield any significant anomaly, neither from C-CTL (Fig. 7g) nor from W-CTL (Fig. 7h). As shown in Figs. 6k-o, ENEA climatology is unable to simulate the latitudinal migration of the ITCZ-WAM system, and also fails in producing the maximum monsoonal rainfall, i.e. located in MJ instead of JAS (also in Losada et al. 2009, this issue). These features could largely explain the diffuse ENEA response; and, since this model does not reproduce the WAM seasonal cycle we will exclude its outputs in the following sections.

In Figure 8 statistical distributions of the MJ and JAS rainfall outputs are displayed in standardized values both model by model (Fig.8a,b), and for the mean-ensemble including all the models (Fig. 8c,d). In order to reduce the systematic errors due to each model, the biases have been considered separately for each model and anomalies with respect to the corresponding model climatology have been computed. The histograms refer to a classification in three categories illustrating the relative occurrences of below normal, quasi normal and above normal situations in warm and cold experiments (see the legend).

In MJ (Fig. 8a,c) there is no significant rainfall difference: no model causes a significant dispersion of the rainfall amounts produced by the cold and warm experiments (circles and asters in 8a, respectively). This is similar when using a model-ensemble approach: the histograms relative to the cold and warm simulations (white and blue bars in Fig. 8c, respectively) are alike. In JAS, at the opposite, the same experiments create contrasted responses, i.e., less (more) rainfall in cold (warm) situations. However, there is a more consistent signal in warm outputs than in cold ones: (i) the latter fail 32.5% in distinguishing the precipitation sign, against only 12.5% in the former (Fig. 8b); (ii) and, considering 4-models together, the cold (warm) experiments model-ensemble generate a ratio of 9/18 (27/2) between excess/deficits (Fig. 8d). Warm situations in the Mediterranean seem therefore to impact more on West African precipitation in contrast with empirical findings,

which showed a symmetrical signal (Figs. 3c,e). For all above, the rest of the work will focus on both the rainy season (JAS) and the forced-response in warm conditions.

5.3 Large-scale wind circulation

Multi-model composites using the anomaly method are now presented for contrasting respectively the 30 cold and 30 warm experiments to the 30 control runs in terms of circulation along the vertical meridional plane (CNRM, UCM, IPSL; excluding ENEA). Figure 9 presents vertical cross sections of wind components (u,v, omega) as simulated by each model averaged along 20°W-30°E where arrows refer to v and omega and contours to the zonal component: left panels display mean control simulations for each model while diagrams at right refer to the significant warm minus control differences tested with a Student t-test at p=0.05. Notice first that several basic elements of the mean monsoon circulation are well simulated by the GCMs (Fig. 9a,c,e), i.e., the monsoon cell southward to 20°N fuelled by air ascents over the Sahel domain and SW winds, the northern overturning circulation, the northern subtropical Westerly Jet in high troposphere and also subsidence over the northern subtropics. However there are some discrepancies with the easterly circulation. For example the African Easterly Jet (AEJ) in mid troposphere is strongly underestimated by UCM and CNRM while IPSL underestimates Tropical Easterly Jet (TEJ) maxima in high levels.

Regarding to the W-CTL model responses, the more significant signals are observed in CNRM and UCM simulations (Fig. 9b,d); i.e., note the unclear circulation in IPSL run (Fig. 9f). As shown in observations (Section 4.2), it can be seen how CNRM experiment produces a significant reinforcement of both the northern and southern Hadley-cells; while UCM only yields the overturning anomaly of the southern meridional circulation. These features reflect the enhancement of the ITCZ activity, according to one of the Rowell's (2003) feedback mechanism which involves reinforced monsoonal circulation (low-level westerlies and rising motion) responding to the enhanced moisture transport from the Mediterranean. An additional northward displacement of this deeper-ITCZ is also apparent: from 10-15N in CTL to 15-20N in W-CTL (Fig. 9). In addition to strengthened southwesterly flow associated with increased latent heat (diabatic heating) in the Sahel region, forced by the above anomalous moisture convergence (Rowell 2003); Peyrillé et al. (2007), by using an idealized 2-D model, have suggested that the poleward extent of continental convection is partially explained by the weakening of the climatological northeasterly flow from the Mediterranean (see below, Section 5.6). Here, in order to gain insight into the proposed mechanism from 3-D AGCM

simulations, figure 10 presents jointly the upper (200hPa, second row) and lower (850hPa, fourth row) streamfunction anomalies. In 850hPa response are apparent the alterations in the local-ITCZ (Figs. 10d,h,l): an anomalous cyclone in the WAM domain at CNRM and UCM forcing deep-upward motions; but an anticyclonic anomaly along Central African Republic and Guinean coastline in IPSL. It is also noticeable the low-level negative anomalies surrounding the eastern Mediterranean basin, associated with negative pressure anomalies there and in accordance with the observational work by Raicich et al. (2003). This feature, the low-level convergence anomaly, would go along with Peyrillé et al. (2007) regarding the decrease of NE winds in response to warming of Mediterranean SST (see Section 5.6); and partially in contrast to Rowell (2003) and Jung et al. (2006) who found no change in the circulation leading to enhanced monsoon precipitation.

Additionally, this anomalous low-level convergent inflow is associated with positive streamfunction anomalies at upper-levels, revealing a baroclinic structure in the atmosphere (Figs. 10b,f,j): along the whole subtropical belt in CNRM, confined into the eastern Mediterranean in UCM, and isolated over the Arabian Peninsula in IPSL. Similar thermally-driven response to changes in the Mediterranean SST has been reported by Li (2006), who found a circumglobal wintertime-teleconnection initiated in the Mediterranean basin. Experiments analyzed here seem to corroborate this direct global-response to Mediterranean summer forcing (García-Serrano et al., manuscript in preparation); while previous evidences support this finding (Jung et al. 2006).

5.5 Moisture fluxes

Figure 11 a,b focuses better on the zonal and meridional mean moisture fluxes in low and mid troposheric layers using all the CNRM runs, i.e, 20 control and 20 warm simulations. Only the CNRM is chosen for taking advantage of the good vertical resolution of this model (45 vertical levels) particularly in low layers (Salas-Mélia et al., 2005). This approach is not extrapolable to other models but it provides valuable insights.

The moisture transport is mainly organized with a SW maximum at 925 hPa by 10°N (positive values in panels a,b) and an easterly maximum at 700 hPa around 10°N, hence just under and southward to the main AEJ axis, as shown by the negative values in Fig 11a. Warm-CTL composites in figure 11c,d present larger significant signals. In particular the zonal moisture transport by the AEJ is shifted northward (negative/positive dipolar patterns at 700 hPa in figure 11c) while in lower levels, negative/positive differences northward/southward to 20°N in figure 11c,d reveal a significant increase of northeasterly and

southwesterly monsoonal flux. This finding implies an enhanced deep convection in the WAM area. Additional analyzes (not reported here) have shown that the increase in northeasterly moisture flux is mainly due to an augmentation of the specific humidity in low-level over the warmer eastern Mediterranean. This strengthens the flux and together with the reinforcement of the southwest monsoon augments moisture convergence in low levels, according to Rowell (2003). This feedback mechanism would also help to the anomalous northward displacement of the ITCZ, providing above-average precipitation over the Sahel.

5.6 Response in low levels

To assess better the capabilities of the 3 models to reproduce correctly the tropical-subtropical circulation over the Mediterranean-African window, figure 12a,c,e displays the mean low level wind fields as produced in the control simulations. The skill of simulations is rather good since several key-elements are reproduced and well located, i.e., Azores and Ste Helena anticyclonic gyres, monsoon and Harmattan systems, ITCZ …

The Warm-CTL significant differences at p=0.10 are presented in figure 12b,d,f with shadings when the v component is positive. The 3 models give anomalous surface westerlies over the Sahelian area, although the location of the signals is different from one model to another. Thus, CNRM concentrates the strongest signals over the Atlantic (under 12°N) and the eastern Sahel, UCM over a large part of the West African continent north to the equator and subtropical Atlantic (12°N-24°N), while IPSL produces significant westerlies in the Sahelian domain but with a similar amplitude south of the equator. Despite these differences, common features emerge from the multi-model approach (Figs. 12g,h). This multi-model ensemble retains large anomalous westerlies coming inland from the Atlantic (Rowell 2003) and reaching the Sahel region, but does not take into account the southerly component from Gulf of Guinea. Additionally, as also shown in each model (Figs. 12b,d,f), the weakening of the climatological northeasterly flow from the eastern Mediterranean is apparent. These anomalous surface winds have a clear southerly component east of 10°E over Egypt. This feature is consistent with the anomalous low-level convergence in the southeastern Mediterranean basin, as discussed above (Figs. 10d,h,l), and is in agreement with Peyrillé et al. (2007) regarding the penetration decrease of the mean circulation depending on the thermal contrast between the African continent and the Mediterranean Sea (or SST-forced in this case).

5.7. Response in mid and high levels

Figures 13 and 14 present the mean and composite wind fields at 600 and 200 hPa, respectively, with shadings where the zonal component is positive (blows eastward). In the top-middle panels are ensemble responses for each model, while in bottom panels are presented the multi-model approach (Figs. 13-14g,h). At 600-200 hPa the control experiment (Figs. 13-14a,c,e) reproduces correctly several specific features of the upper and mid level circulation, i.e., the AEJ and TEJ main axes over West Africa, the subtropical westerly jet pattern over the Mediterranean, and at 600 hPa northerlies from the Mediterranean. Warm experiments (Figs. 13-14b,d,f) cause (i) a significant reduction of subtropical westerlies in high levels south of the equator; (ii) a significant increase in TEJ, more clearly seen in each model behaviour than multi-model ensemble, confined to 0°E and 15°E; and (iii) a relative decrease in AEJ, with clear distinct location in each model which causes a diffuse signal in the multi-model ensemble. All of these features are known to be favourable to the monsoon circulation (Newell and Kidson 1984; Fontaine et al., 1995).

6. Discussion and conclusion

The purpose of this study was twofold: (i) reexamining the observed relationship between the Mediterranean thermal variability (Western and Eastern basins) and Sudan-Sahel rainfall estimates over the recent period, i.e., not marked by long wet and dry phases (as in the 50-70s); (ii) reporting some rainfall and atmospheric impacts generated by warm JAS anomalies in the Mediterranean Basin using multi-model sensitivity experiments. The results provide from both empirical and numerical ensemble approaches. The analyses use 3 types of datasets: in situ observations (rainfall, sea surface temperature…), satellite estimates (GPCP, CMAP data) and reanalyzed data from the NCEP-DOE AMIP II (winds and specific humidity on isobaric surfaces …).

Considered together the statistical and numerical results let suppose the existence of a thermal forcing of the Mediterranean on the African monsoon. Basically Mediterranean warming, with maximum amplitude in the eastern basin, leads to enhanced moisture convergence and therefore rainfall over Sudan-Sahel latitudes in agreement with Rowell (2003) who reports also a strengthening of moist advection across the Eastern Sahara by the mean flow. Peyrillé et al. (2007) insist more on a reduction of northerlies both in magnitude and extension, compatible with a deeper northward migration of the ITCZ into the continent. In accordance with the latter, Raicich et al. (2003) evidenced that the Sahel monsoonal season

is associated with below-normal surface pressure in the eastern Mediterranean. All above has been also verified here, implying that this Mediterranean-WAM connection was robust during recent decades. Thus, when the warming concerns the East basin, a strong link with Sahel precipitation has been found, involving the reinforcement of both the ITCZ-deep motion and westerly transport of humidity thereby, in short, strengthening the main WAM circulation regime. An open question to be addressed concerns the WAM teleconnection with the West basin. Our observational analysis suggests a relationship with deep convection over Gulf of Guinea, possibly related to the Atlantic equatorial SST mode.

The empirical results allowed us to discuss the linearity and significance of the relationship. They can be summarized in 3 points.

(1) The Eastern Mediterranean concentrates the highest SVD temperature variance, while a large continental region, located somewhat northward to the mean ITCZ position, accumulates the strongest loadings in terms of enhanced deep convection and ascendance. This connection has been found in both synchronous and one month-lead performances, suggesting an important influence of the East basin on the WAM system.

(2) Additional results have confirmed the existence of a one month delay between thermal variability in the Mediterranean and deep convection over Africa. There are also preferred time scales for correlations, i.e., synoptic variability (< 10 days) and AEWs (3-5 days). This last connection is mainly observed eastward to the 0° longitude, a region known for a long time as an area of AEW development. These features will be also further analysed in the future through AGCMs and WRF simulations.

(3) When the Eastern basin is abnormally warm the northward migration of the monsoon system and ascendances around the ITCZ reinforce through deeper moist convection south of the Sahara. These air ascents strengthen northerlies at 200 hPa and hence the monsoon cell, air descents above the Southern Tropics and low level moist winds from the South. This increases moisture transport under 400 hPa over the continent (5°N-20°N), low level convergence via the SW monsoonal flow in the Sahel zone and hence rainfall surplus just northward to the rain belt in July-September. Additional analyses (not produced here) and figure 3 show that the reverse tends to occur in cold situations, in accordance with Rowell (2003).

The *SST sensitivity experiments* linked to normal, warm and cold situations over the Mediterranean and performed on four AGCMs allowed us first to illustrate the relative good

accuracy of the models to reproduce the May to September evolution of several key-elements of the monsoon circulation. The more reliable latitudinal-migration of the rainbelt climatology has been found for CNRM and UCM models.

Second, in the models the response between warm and cold situations in the Eastern Mediterranean is not symmetric: the sensitivity experiments showed that warm occurrences impact more on West African precipitation than cold ones. In fact, cold-SST runs have not been conclusive, becoming separated from the linear hypothesis of Rowell (2003). Perhaps, it is because of the AGCM difficulty for well simulating the reduced-latent heat release in cold situations. It is also important to mention that climatological summer SST conditions in the Mediterranean Sea resemble a zonal gradient with maximum located in the eastern basin quite similar to forcing fields prescribed in the simulations (not shown). Hence, the Mediterranean-Sahel connection in cold conditions continues being an issue to be explored. By contrast, the positive empirical relationship between warm SSTs in the Mediterranean and the West African monsoon can be interpreted in terms of thermal Mediterranean forcing.

In this way, warm experiments generate an enhancement of the southern meridional cell in low and high levels, related to reinforced monsoonal southwesterlies, a more northward location of its ascending branch (ITCZ) over West Africa in association with more (less) intense monsoon and TEJ (AEJ). It is however important to bear in mind that such changes in the overturning circulation are not necessarily directly forced by Mediterranean SST since the enhanced moisture transport from the Mediterranean into the Sahel region increases also the latent heat and diabatic heating. This tends to fuel the rising motion in the WAM area and subsequently the downward motion in the overturning circulation.

An integrating picture has been evidenced from AGCM simulations presented here. According to Rowell (2003) and Fontaine et al. (2003), the favoured humidity transport from the Mediterranean Sea into ITCZ is accompanied by both anomalous surface-influx from the tropical Atlantic and reduced export via AEJ at mid-levels (two of the Rowell's feedbacks). The former could help to displace more northward the WAM-deep convection up to the Sahelian region. In addition, another mechanism has been shown contributing to this anomalous poleward ITCZ-extension. Consistent with the lower-tropospheric convergence found in the southeastern Mediterranean basin, which could explain the surface pressure anomalies suggested by Raicich et al. (2003), is the weakening of the climatological northeasterly flow east of 10°E over Egypt. This finding is in agreement with the penetration

decrease of the mean circulation depending on the thermal contrast between African continent and the Mediterranean Sea (or SST-forced in the simulations; Peyrillé et al. 2007). This feature reflects a substantial northward migration of the monsonal rainbelt, and hence above-normal precipitation over the Sahel. This result does not contradict the anomalous moisture transport originated in the Mediterranean; since although weakened, the additional evaporation would be advected southward across the eastern Sahara by the flow.

Acknowledgements: The authors are very grateful to the anonymous reviewers for their interesting comments, and to the National Center for Atmospheric Research (USA), Climate Prediction Centers and the National Oceanic and Atmospheric Administration for providing the data. J. G.-S. greatfully acknowledge the founds from the ESF-MedCLIVAR Programme of grants (EG/1694). The study was mainly supported by the Global change and Ecosystems programme (EU Integrated project: African Monsoon Multidisciplinary Analysis (AMMA) and the French component of AMMA. Based on a French initiative, AMMA was built by an international scientific group and is currently funded by a large number of agencies, especially from France, UK, US and Africa. It has been the beneficiary of a major financial contribution from the European Community's Sixth Framework Research Programme. Detailed information on scientific coordination and funding is available on the AMMA International web site http://www.amma-international.org

References

Adler, R. F., Huffman , G. J., Chang, R., Ferraro, A., Xie, P., Janowiak, J. E., Rudolf, B., Schneider, U., Curtis, S., Bolvin, D. T., Gruber, Susskind, J. and Arkin, P., The version 2 Global Precipitation Climatology Project (GPCP) monthly precipitation analysis (1979-present), *J. Hydrometeor*, *4* (6), 1147-1167, 2003.

Fontaine B., Janicot S. and Moron V, Rainfall anomaly patterns and wind field signals over West Africa in August (1958-1989), *Journal of Climate*, 8, 6, 1503-1510, 1995.

Fontaine B., Roucou P. and Trzaska S., Atmospheric water cycle and moisture fluxes in the West African monsoon: mean annual cycles and relationship using NCEP/NCAR reanalyses , Geophys. Res. Lett., 30, 3, 10.1029-10.1032, 2003.

Hall N.M.J. and P. Peyrillé, Dynamics of the West African Monsoon. J. Phys. IV, France, 139, 81-99. © EDP Sciences, Les Ulis. DOI: 10.1051/jp4:2006139007, 2006.

Joly M., Rôle des oceans dans la variabilité vclimatique de la mousson ouest africaine, PhD dissertation, 200 pages, CNRM/GAME, Météo-France, Toulouse, 2008

Kanamitsu, M., Ebisuzaki, W., Woolen, J., Yarg, S.-K., Hnilo, J. J., Fiorino, M. and Potter, G. L., NCEP-DOE AMIP-II reanalysis (R-2), *Bulletin of American Meteorological Society*, *83*, 1631-1643, 2002.

Li, L.Z.X., Atmospheric GCM response to an idealized anomaly of the Mediterranean sea surface temperature. *Clim Dyn*, **27**, 543-552, 2006.

Louvet S, Fontaine B, Roucou P., Which rainfall dataset can be used to study African monsoon at intra-seasonal timescale? Technical Note, 3 tables, 10 figures, 27 pages. CRC, Dijon, 2007.
http://www.ubourgogne.fr/climatologie/AMMA_D1.1.3/other_rainfall_product.htm

Jung, T, Ferranti, L, and Tompkins A.M., Response to the Summer of 2003 Mediterranean SST Anomalies over Europe and Africa, *J. Clim.*, 2006, 19, 20, 5439-5454, 2006.

Mitchell TD, Carter TR, Jones PD, Hulme M, New M. 2004. A comprehensive set of high-resolution grids of monthly climate for Europe and the globe: the observed record (1901-2000) and 16 scenarios (2001-2100). Tyndall Working Paper 55, Tyndall Centre, UEA, Norwich, UK. http://www.tyndall.ac.uk/

New M, Lister D, Hulme M, Makin I, A high-resolution data set of surface climate over global land areas. Climate Research 21: 1–25, 2002.

Murakami, M., Large scale aspects of deep convective activity over the Gate area, *Monthly Weather Review*, *107*, 994-1013, 1979.

Newell, R. E. and J. E. Kidson, African mean wind changes between Sahelian wet and dry periods, *J. Climatol.*, 5, 27-33, 1984.

Peyrillé P., J. P. Lafore, J. L. Redelsperger, An idealized two-dimensional framework to study the West African Monsoon. Part I: validation and key controlling factors, *J. Atmos. Sci.*, , 64, 2765-2782, 2007.

Peyrillé P., and J. P. Lafore, An idealized two-dimensional framework to study the West African Monsoon. Part II: large-scale advection ansd the diurnal cycle, *J. Atmos. Sci.*, , 64, 2783-2803, 2007.

Polo I., B. Rodríguez-Fonseca, T. Losada and J. García-Serrano, Tropical Atlantic Variability modes (1979-2002). Part I: time-evolving SST modes related to West African rainfall. *J. Climate*, DOI: 10.1175/2008JCLI2607.1, 2008 (in press).

Raicich, F., N. Pinardi and A. Navarra, Teleconnections between Indian monsoon and Sahel rainfall and the Mediterranean. *Int. J. Climatol.* **23**, 173–186, 2003.

Rodwell, M. J. and B. Hoskins, Monsoons and the dynamics of deserts. *Q. J. R. Meteorol. Soc.*, **122**, 1385-1404, 1996.

Rowell D.P., The Impact of Mediterranean SSTs on the Sahelian Rainfall Season. *J. Clim.*, 16, 849-862, 2003.

Salas-Mélia, D., F. Chauvin, M. Déqué, H. Douville, J.F. Gueremy, P. Marquet, S. Planton, J.F. Royer and S. Tyteca (2005) : Description and validation of the CNRM-CM3 global coupled model, CNRM working note 103., available at
http://www.cnrm.meteo.fr/scenario2004/references_eng.html

Xie, P. and Arkin, P. A., Global precipitation: a 17-year monthly analysis based on gauge observations, satellite estimates, and numerical model outputs, *Bull. Amer. Meteor. Soc.*, *78*, 2539-2558, 1997.

Xie, P., Janowiak, J. E., Arkin, P. A., Adler, R. F., Gruber, A., Ferraro, R., Huffman, G. J. and Curtis, S., GPCP pentad precipitation analyses: An experimental dataset based on gauge observations and satellite estimates, *Journal of Climate*, *16*, 2197–2214, 2003.

Yin, X., Gruber, A. and Arkin, P. A., Comparison of the GPCP and CMAP merged gauge satellite monthly precipitation products for the period 1979-2001, *Journal of Hydrometeorology*, *5*, 1207-1222, 2004.

Tables

15°W-30°E	**JAS**	**M**	**J**	**J**	**A**	**S**	**O**
North Africa: 05°N-20°N							
Mean rainfall amounts (mm)	410	66	95	136	159	115	59
W-C West Medit	+6%	-13%	-11%	-2%	*+15%* *	+4%	+15%
W-C East Medit	+11%	***-22%*** **	-2%	+4%	+13%	+17%	+11%
Sahelian belt: 13°N-18°N							
Mean rainfall amounts (mm)	219	8	27	73	101	44	8
W-C West Medit	+16%	-22%	-21%	+12%	+24%	+3%	+55%
W-C East Medit	***+22%*** **	*-44%* *	+3%	*+18%* *	+17%	***+39%*** **	+44%

Table 1: Observed relationship between Mediterranean surface temperatures and North African (5°N-20°N) and Sahel (13°N-18°N) rainfall amounts averaged between 15°W and 30°E for the seasons July-September (JAS) and the months May to October. Mean rainfall amounts in mm and warm minus cold differences (W-C) in percentages relative to the western and eastern Mediterranean basins. Period 1979-2002.
The warmest Mediterranean summers are 1987, 1989, 1990, 1991, 1994, 1999, for the Western basin and 1988, 1994, 1998, 2000, 2001, for the eastern basin The coldest ones are 1979, 1980, 1981, 1984, 1993, 1996, 1997, 2002 for the western basin and 1979, 1981, 1983, 1984, 1991, 1992, 1996, 1997 for the eastern basin. The significant values at p=0.1 (*) and 0.05 (**) using a Student t-test are indicated in italic and bold, respectively.
Underlined values means that differences are significant with a null hypothesis that the East and West Mediterranean have the same relationship with rainfall'.

	Unfiltered series				Filtered series : variability < 8 years			
	West Medit.		East Medit		West Medit.		East Medit	
	CMAP	GPCP	CMAP	GPCP	CMAP	GPCP	CMAP	GPCP
WSAH	+07	*+38*	+15	***+65***	+16	+30	***+42***	***+63***
CSAH	+24	+29	***+47***	***+57***	***+41***	***+50***	***+65***	***+66***
ESAH	+18	+10	+31	+37	***+52***	***+44***	***+73***	***+66***
CSUD	-13	***+42***	+01	***+59***	+21	***+42***	***+58***	***+62***

Table 2: Correlation coefficients between July-September surface temperatures in the Western / Eastern Mediterranean and July-September CMAP and GPCP rainfall estimates averaged over western Sahel (WSAH), central Sahel (CSAH), Eastern Sahel (ESAH) and central Sudan (CSUD) with and without time filtering. The significant values at p=0.1, 0.05 and 0.01 taking into account time autocorrelations in the series are indicated in italic, bold and underlined, respectively. Period 1979-2006

T, OLR, days	**With trend**	detrended	3-5d	<10d	10-90
% cov/var	**11.5**	17	10.7	8.5	9.9
% SVD1	**51.9**	29	46.2	45.6	43.9
Corr SVD1	**+51**	+42	+48	+41	+26

Table 3: Percentages of covariance and covariance fractions explained by the leading July-September mode (SVD1) at a daily timescale and time correlations (Corr SVD1) with and without linear trend (detrend) and as a function of time filtering in different ranges for capturing the 3-5 day (AEWs), < 10-day (synoptic), 10-90 day (intraseasonal) variability over the period 1979-2006.

Figure Captions

Figure 1: First and second leading July to September SVD modes performed between skin temperatures in the Mediterranean region and West African OLR values at monthly time step: a,b (d,e) describe the first (second) mode in terms of heterogeneous field of covariability and expansion time coefficients while c displays lead/lag correlation coefficients between a spatial index averaging surface temperatures in the Mediterranean basin (32°N-40°N; 6°W-36°W) and OLR values in the Sahel zone (10°N-20°N; 15°W-30°E). Values significant at p=0.05 taking into account autocorrelations in the series are marked by asters. Period July-September 1979-2006

Figure 2: Monthly evolution of the 1st SVD heterogeneous mode between skin temperature in the Mediterranean region and one-month lagged WAM OLR anomalies; spatial domains as in Fig. 1. The respective covariance fractions in % of total variance are indicated. Period 1979-2006.

Figure 3: Warm and cold composites of OLR fields in July-September: **(a)** mean field; **(b)** and **(c)** differences between the warmest situations and all the others relative to the Western and Eastern Mediterranean, respectively; **(d)** and **(e)** as above but for the coldest situations.

The warmest JAS seasons are 1987, 1989, 1990, 1991, 1994, 1999, 2003, 2006 for the Western basin and 1988, 1994, 1998, 2000, 2001, 2003, 2005, 2006 for the eastern basin

The coldest ones are 1979, 1980, 1981, 1984, 1993, 1996, 1997, 2002 for the western basin and 1979, 1981, 1983, 1984, 1991, 1992, 1996, 1997 for the eastern basin.

The shadings refer to OLR values < 240 W/m2 with a 5 W/m2 increment (in a) and to the significant signals at p=0.1 using a Student t-test (in b-e). Period 1979-2006.

Figure 4: July-September mean meridional/vertical cross sections and composites of wind and specific humidity along the 20W-0° (left) and 0°-30°E (right) meridional planes: **(a)** and **(b)**: mean circulation; **(c,d)** warm composites relative to the Western Mediterranean; **(e,f)** warm composites relative to the Eastern Mediterranean. In **(a,b)** the shadings points to the layer where specific humidity > 10g/Kg; in **(c-f)**, red arrows and shadings refer to the significant signals in wind and specific humidity at p=0.1, respectively, after using a Student t-test. Period 1979-2006.

Figure 5: May to October forcing fields used in the AGCM-sensitivity experiments. SST anomalies are expressed in ºC units.

Figure 6: May to September mean monthly rainfall fields from the CPC merged precipitation **(a-e)** on the period 1979-1988 and from the control experiments of each model CNRM **(f-j),** ENEA **(k-o),** IPSL **(p-t)** and UCLA **(u-y)**. Isolines from 2 to 10 mm/day; shadings for values > 6 mm/day.

Figure 7 : Cold minus Control and Warm minus Control rainfall differences in May-June **(left part)** and July-September **(right part)** for the different GCMs: red/blue curves for positive/negative anomalies; shadings are superimposed when differences are significant at p=0.05 regarding a paired-t-test.

Figure 8: (**Top**) Simulated rainfall anomalies (vs control) of the West African Index (20W-30°E; 5°N-20°N) in standardized values for each GCM: May-June **(a)** and July-September **(b):** circles and asters for cold and warm experiments.
(**Bottom**) distributions into 3 classes of the model-ensemble responses relative to the cold and warm (thin bars) experiments : 1=deficits (< -0.5 std), 2=normal and 3=excess (> 0.5 std).

Figure 9: July-September vertical-meridional cross sections of the 3-D wind field modeled by CNRM (**top**), UCM and IPSL (**bottom**) after averaging the results between 20°W and 30°E. Arrows refer to the v and omega components and isolines to the u component. Red/black contours each 2 m/s for positive/negative u values. **Left** :control runs. **Middle**: Cold minus control differences with shadings when the zonal wind is positive. **Right**: Warm minus control differences. Arrows and shadings for significant signals from a paired-t-test at p=0.05.

Figure 10: July-September streamfunction composite at 200hPa (first and second rows) and 850hPa (third and fourth rows) from CNRM (**left**), UCM (**middle**) and IPSL (**right**). **First** (ci=1.0 x 10^7 m^2/s) and **Third** (ci=3.0 x 10^6 m^2/s) rows: control runs. **Second** (ci=0.8 x 10^6 m^2/s) and **Fourth** (ci=0.3 x 10^6 m^2/s) rows: warm experiments. Here the shadings refer to significant differences regarding a Student t-test at p=0.05.

Figure 11: July-September vertical-meridional cross sections of mean and composite moisture fluxes from CNRM over the longitudinal window 20°W-30°E. (**a,b**): u and v mean components from the control runs; (**c,d**): composite differences between the warm and control simulations. The solid (dashed) contours refer to the positive (negative) differences. In panels **c-d**, shadings are superimposed when composite differences are significant at p=0.10 regarding a Student t-test.

Figure 12: Top: July-September mean wind fields in low levels (925 hPa) from CNRM (**left**)**,** UCM (**middle**) and IPSL (**right**) experiments; control runs with positive meridional wind shaded. **Middle**: Warm minus control differences. Here the shadings refer to significant differences regarding a Student t-test at p=0.10. **Bottom:** Multi-model ensemble of wind (arrows) and horizontal divergence (contours) fields at 950 hPa; mean (**left**) and Warm minus Control composite (**right**). Red arrows are superimposed when the differences on panel h are significant at p=0.10 regarding a Student t-test. Contours refer to the positive (negative) differences in divergence.

Figure 13: As Fig. 12 but for horizontal flow at 600 hPa. Shading underline positive values.

Figure 14: As Fig. 12 but for horizontal flow at 200 hPa. Shadings underline positive values.

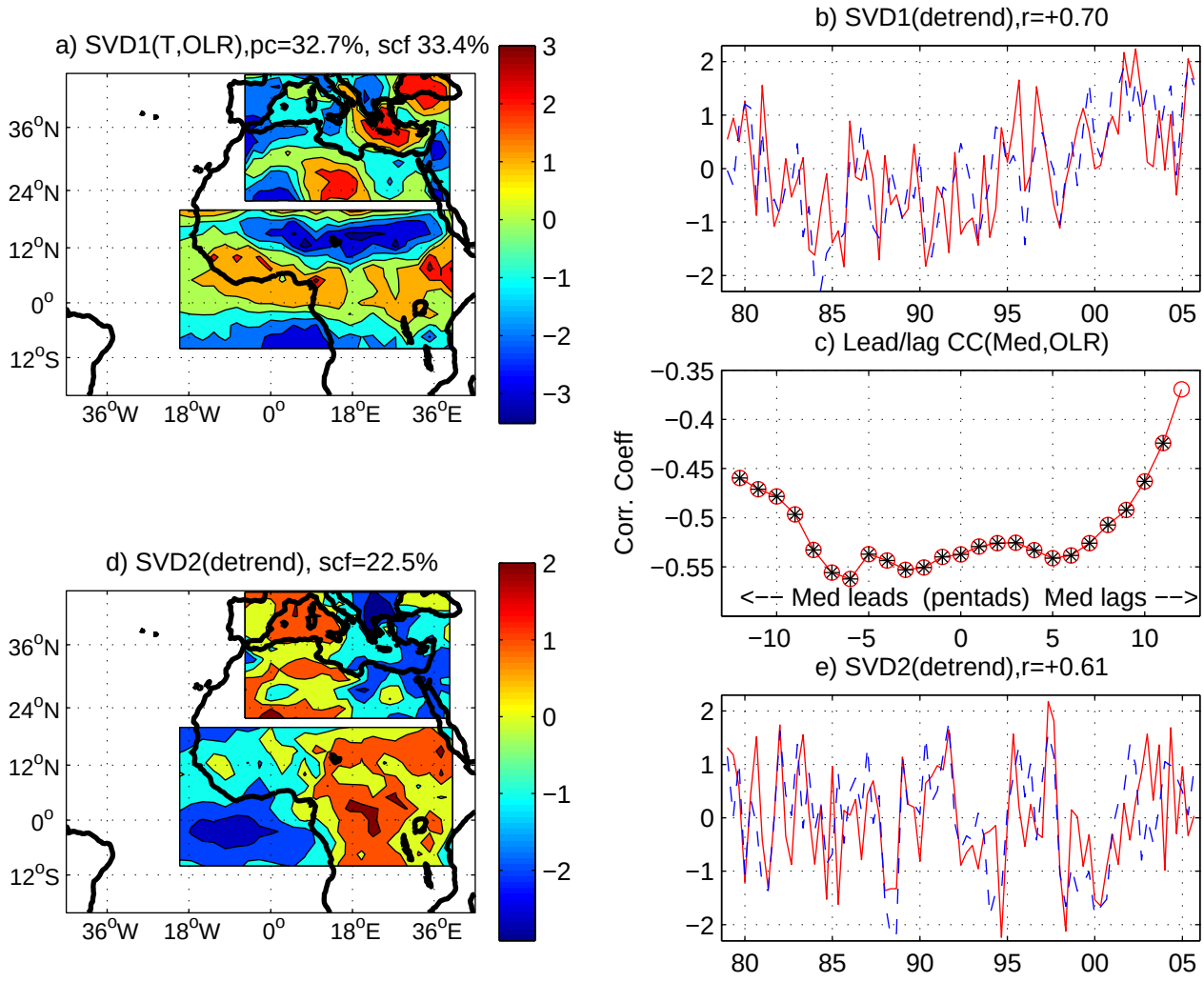

Figure 1: First and second leading July to September SVD modes performed between skin temperatures in the Mediterranean region and West African OLR values at monthly time step: a,b (d,e) describe the first (second) mode in terms of heterogeneous field of covariability and expansion time coefficients while c displays lead/lag correlation coefficients between a spatial index averaging surface temperatures in the Mediterranean basin (32°N-40°N; 6°W-36°W) and OLR values in the Sahel zone (10°N-20°N; 15°W-30°E). Values significant at p=0.05 taking into account autocorrelations in the series are marked by asters. Period July-September 1979-2006

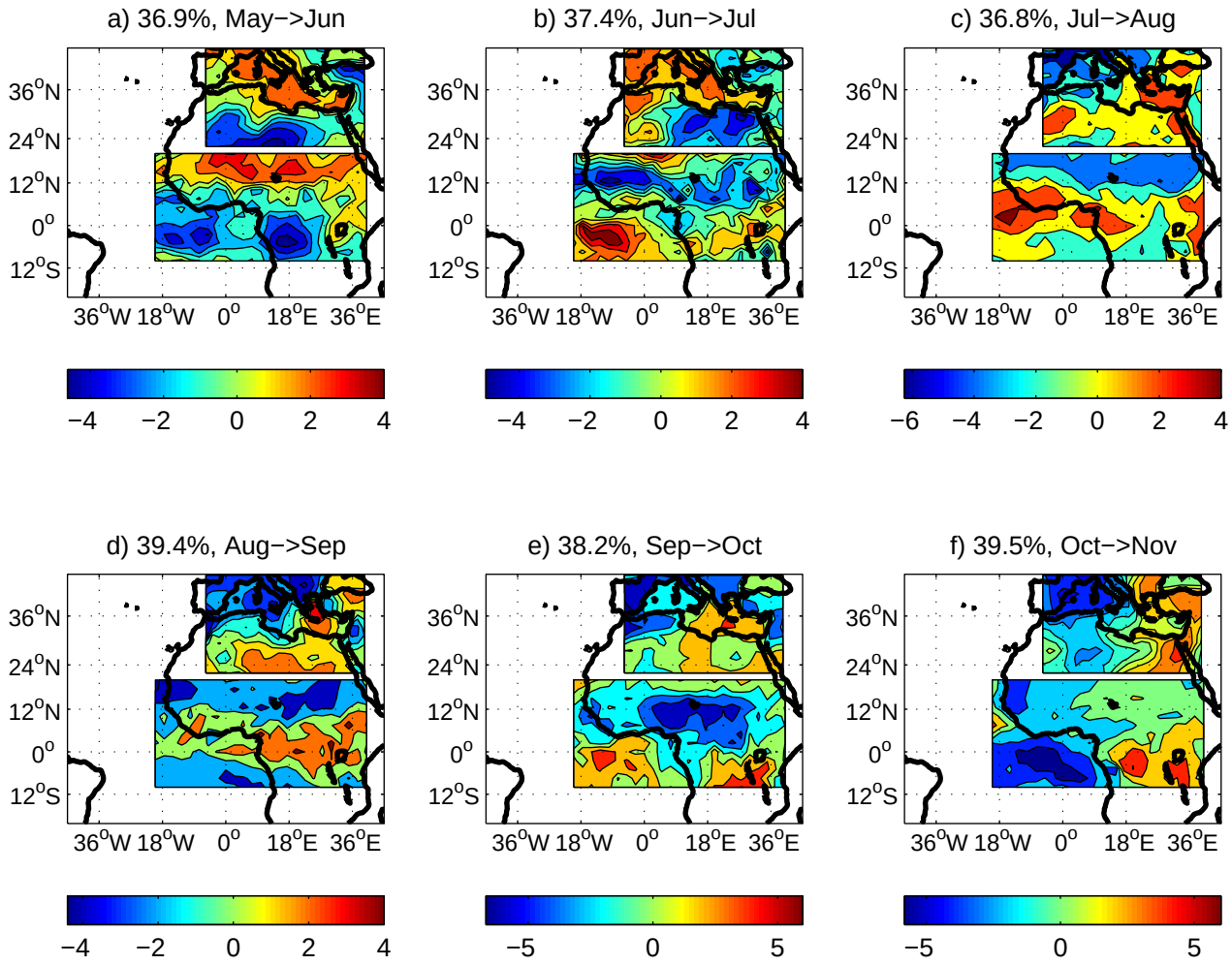

Figure 2: Monthly evolution of the 1st SVD heterogeneous mode between skin temperature in the Mediterranean region and one-month lagged WAM OLR anomalies; spatial domains as in Fig. 1. The respective covariance fractions in % of total variance are indicated. Period 1979-2006.

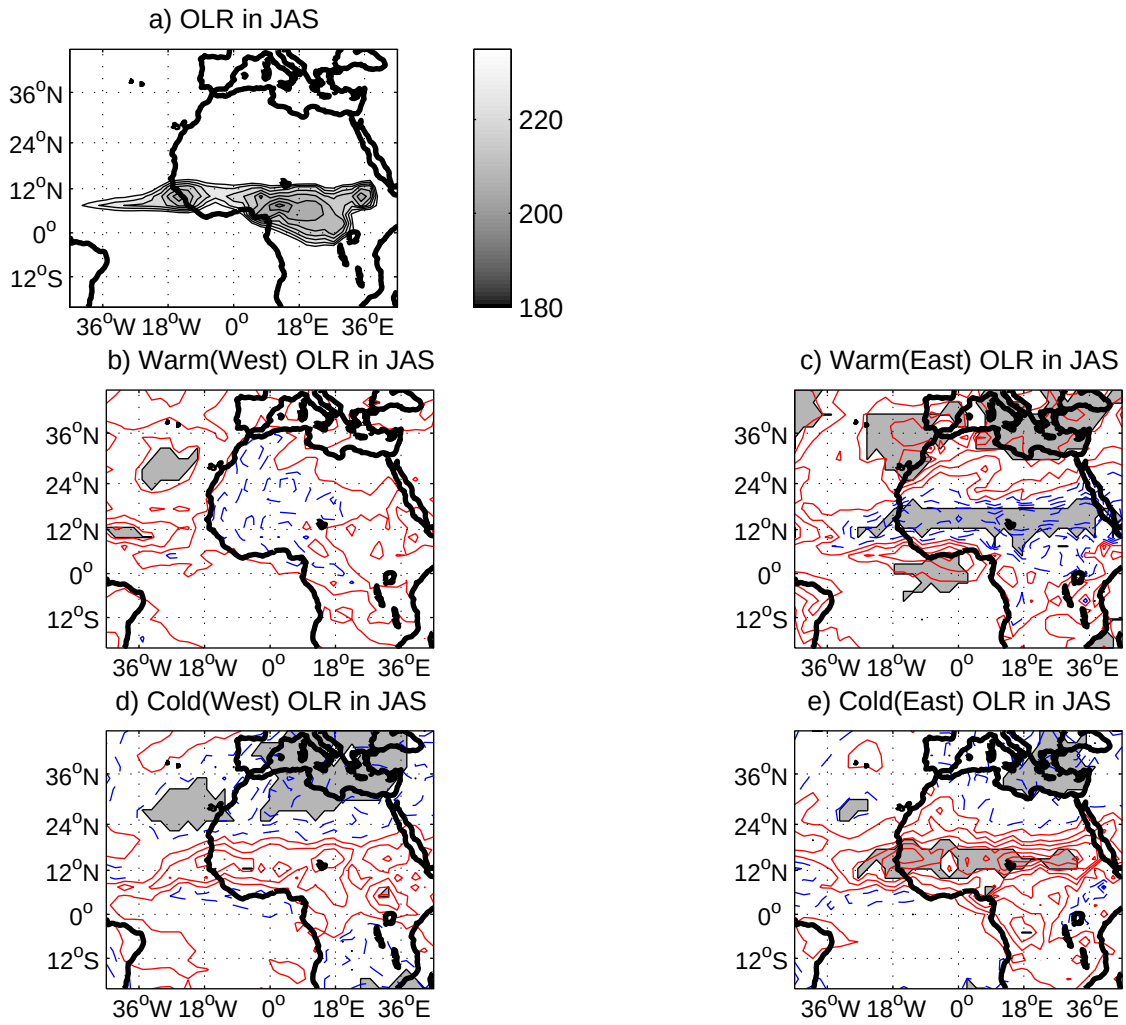

Figure 3: Warm and cold composites of OLR fields in July-September: **(a)** mean field; **(b)** and **(c)** differences between the warmest situations and all the others relative to the Western and Eastern Mediterranean, respectively; **(d)** and **(e)** as above but for the coldest situations.

The warmest JAS seasons are 1987, 1989, 1990, 1991, 1994, 1999, 2003, 2006 for the Western basin and 1988, 1994, 1998, 2000, 2001, 2003, 2005, 2006 for the eastern basin

The coldest ones are 1979, 1980, 1981, 1984, 1993, 1996, 1997, 2002 for the western basin and 1979, 1981, 1983, 1984, 1991, 1992, 1996, 1997 for the eastern basin.

The shadings refer to OLR values < 240 W/m2 with a 5 W/m2 increment (in a) and to the significant signals at p=0.1 using a Student t-test (in b-e). Period 1979-2006.

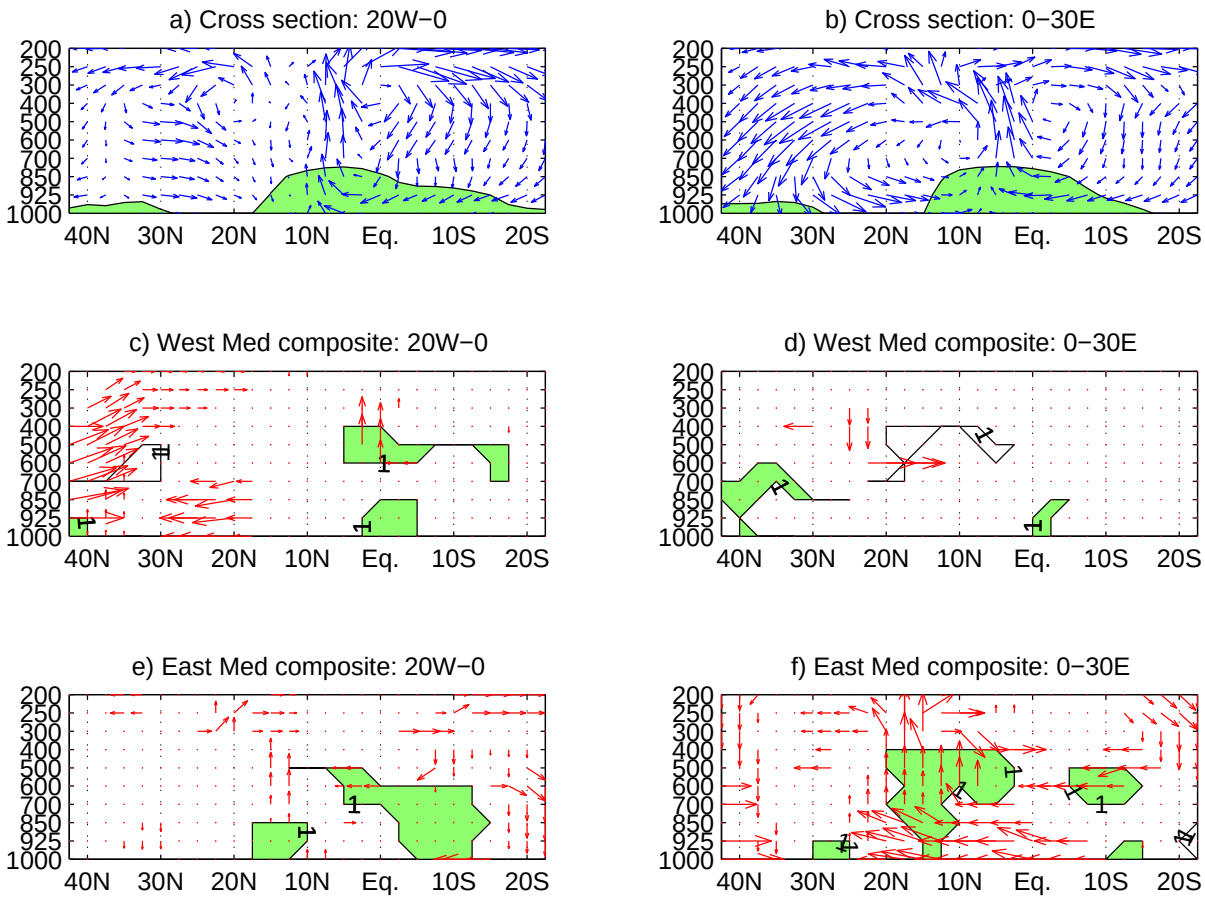

Figure 4: July-September mean meridional/vertical cross sections and composites of wind and specific humidity along the 20W-0° (left) and 0°-30°E (right) meridional planes: **(a)** and **(b)**: mean circulation; **(c,d)** warm composites relative to the Western Mediterranean; **(e,f)** warm composites relative to the Eastern Mediterranean. In **(a,b)** the shadings points to the layer where specific humidity > 10g/Kg; in **(c-f)**, red arrows and shadings refer to the significant signals in wind and specific humidity at p=0.1, respectively, after using a Student t-test. Period 1979-2006.

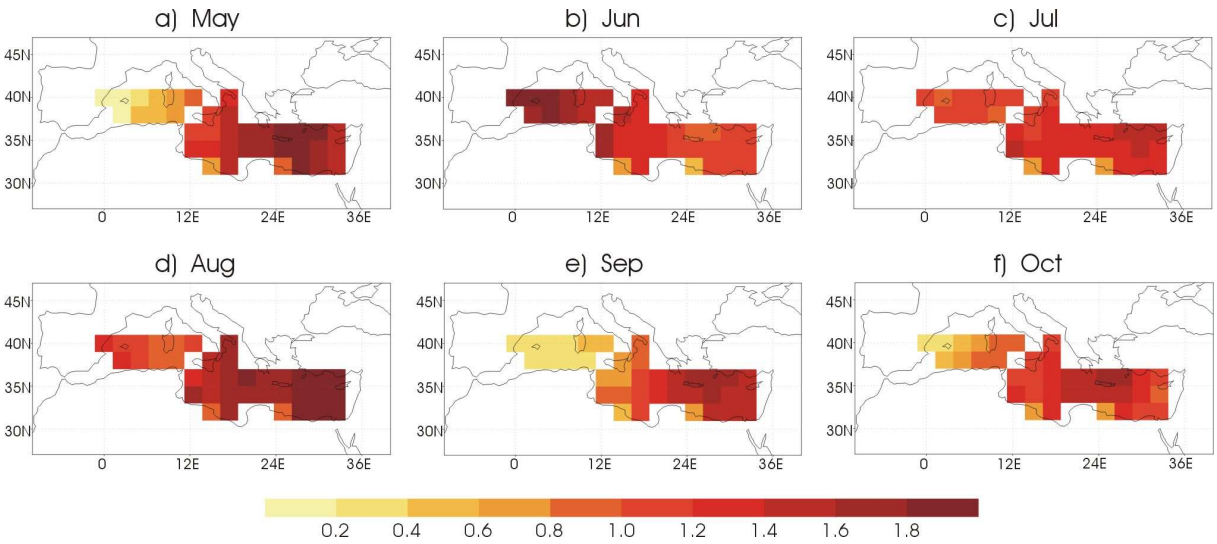

Figure 5: May to October forcing fields used in the AGCM-sensitivity experiments. SST anomalies are expressed in ºC units.

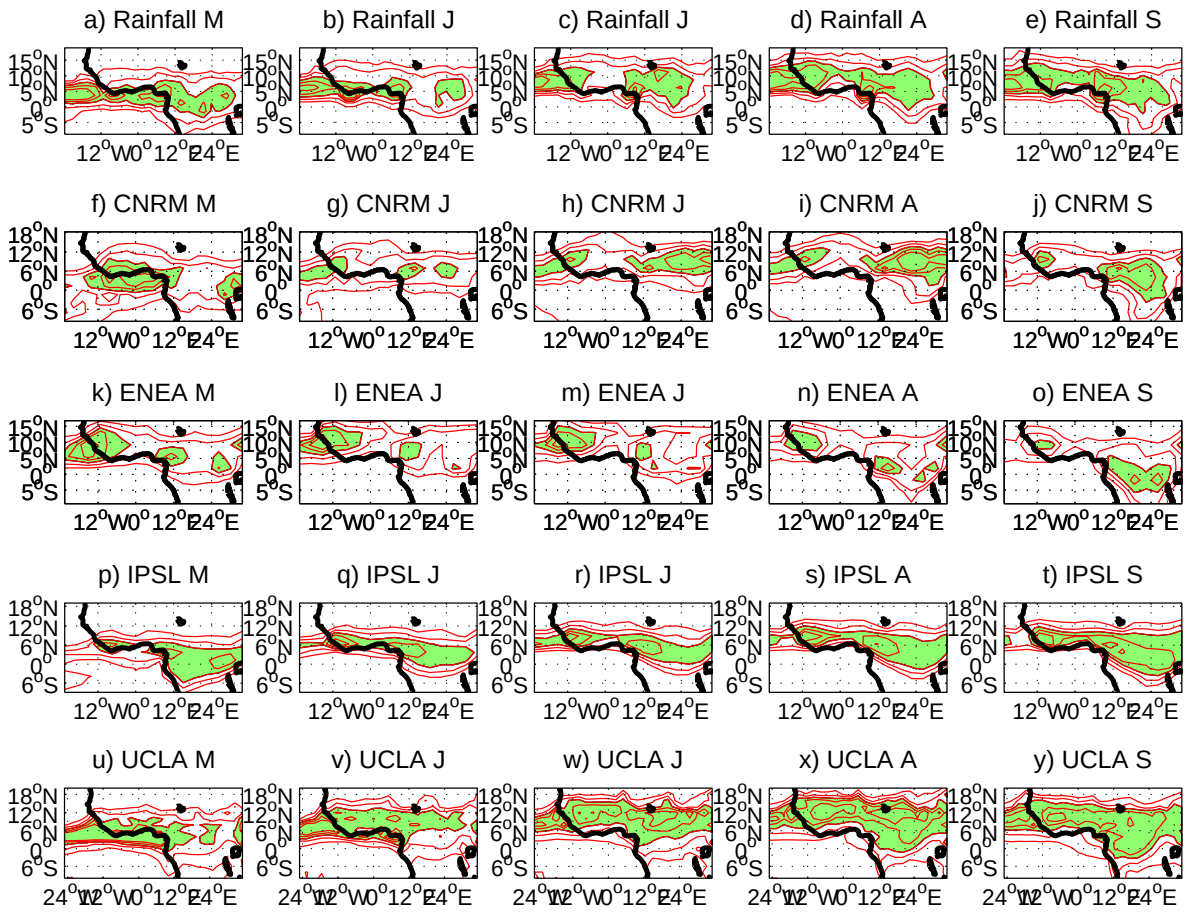

Figure 6: May to September mean monthly rainfall fields from the CPC merged precipitation **(a-e)** on the period 1979-1988 and from the control experiments of each model CNRM **(f-j),** ENEA **(k-o),** IPSL **(p-t)** and UCLA **(u-y)**. Isolines from 2 to 10 mm/day; shadings for values > 6 mm/day.

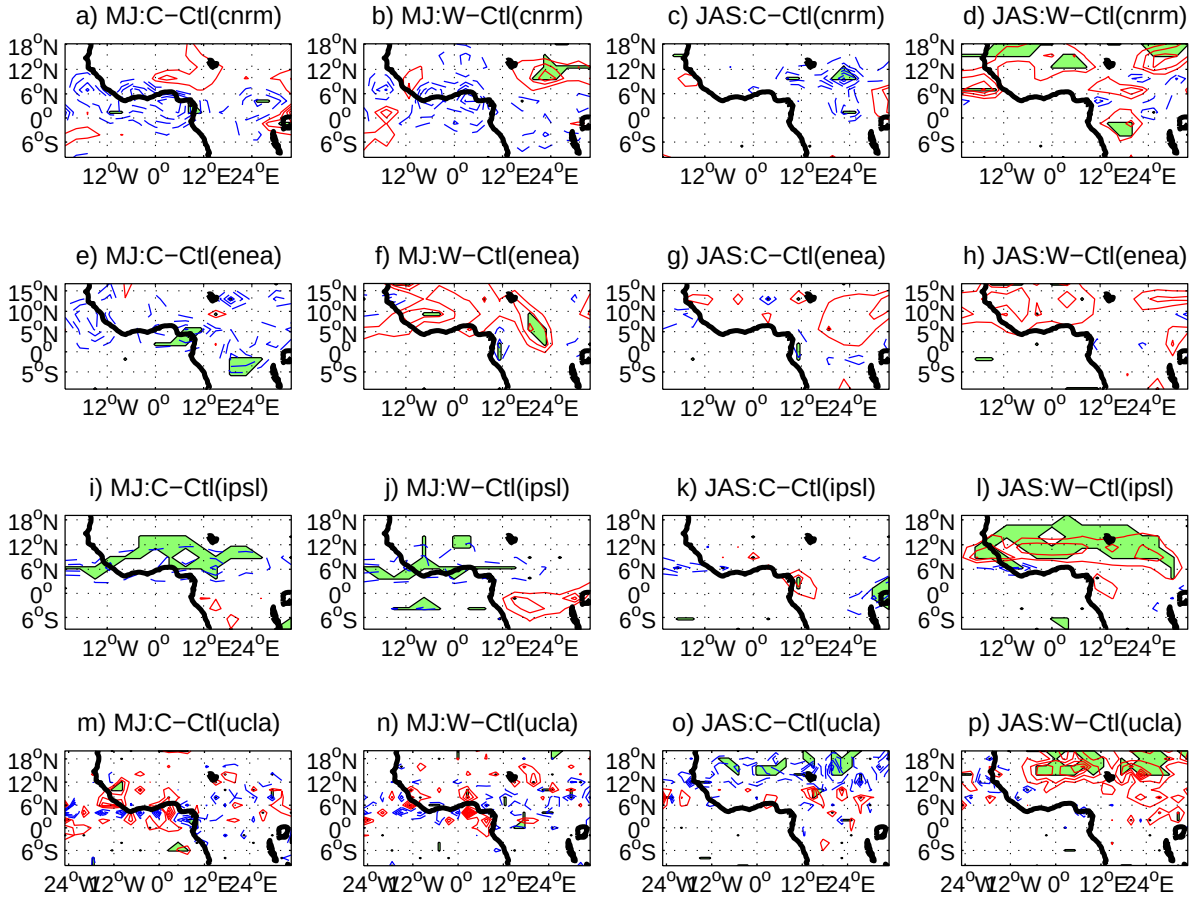

Figure 7 : Cold minus Control and Warm minus Control rainfall differences in May-June (**left part**) and July-September (**right part**) for the different GCMs: red/blue curves for positive/negative anomalies; shadings are superimposed when differences are significant at p=0.05 regarding a paired-t-test.

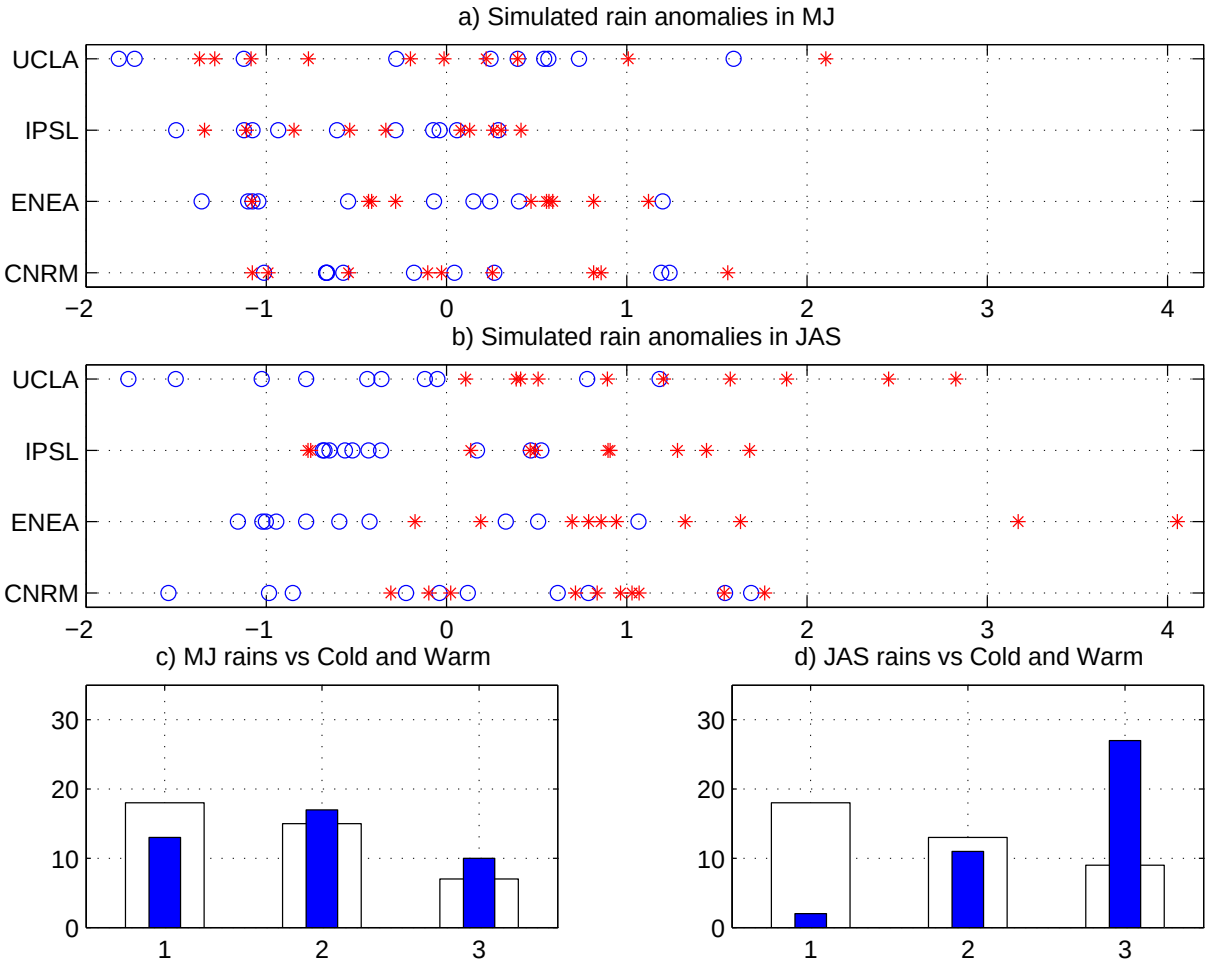

Figure 8: Top: Simulated rainfall anomalies (vs control) of the West African Index (20W-30°E; 5°N-20°N) in standardized values for each GCM: May-June (**a**) and July-September (**b**): circles and asters for cold and warm experiments. **Bottom**: Distributions into 3 classes of the model-ensemble responses relative to the cold and warm (thin bars) experiments : 1=deficits (< -0.5 std), 2=normal and 3=excess (> 0.5 std).

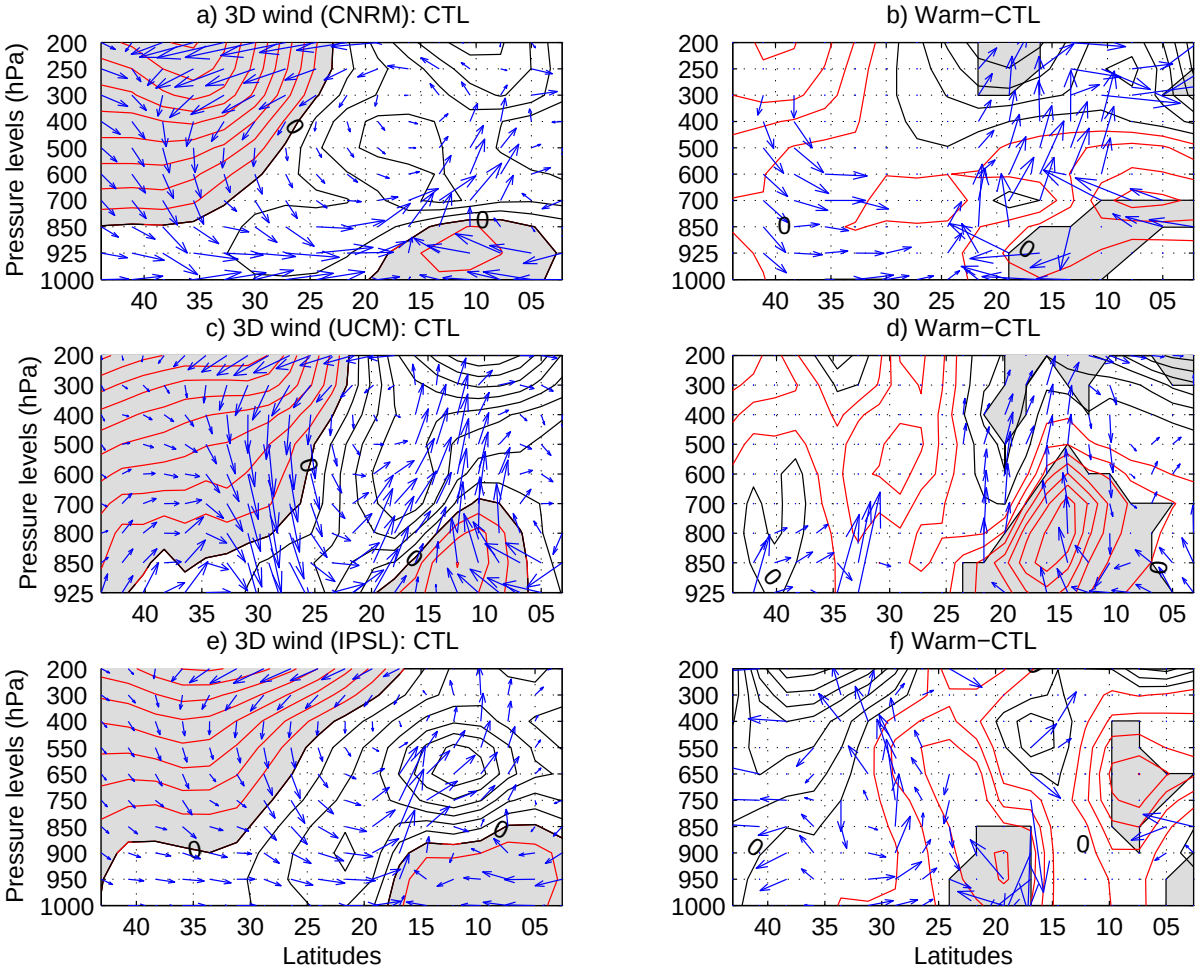

Figure 9: July-September vertical-meridional cross sections of the 3-D wind field modeled by CNRM (**top**), UCM and IPSL (**bottom**) after averaging the results between 20°W and 30°E. Arrows refer to the v and omega components and isolines to the u component. Red/black contours each 2 m/s for positive/negative u values. **Left** :control runs. **Right**: Warm minus control differences. Arrows and shadings for significant signals from a paired-t-test at p=0.05.

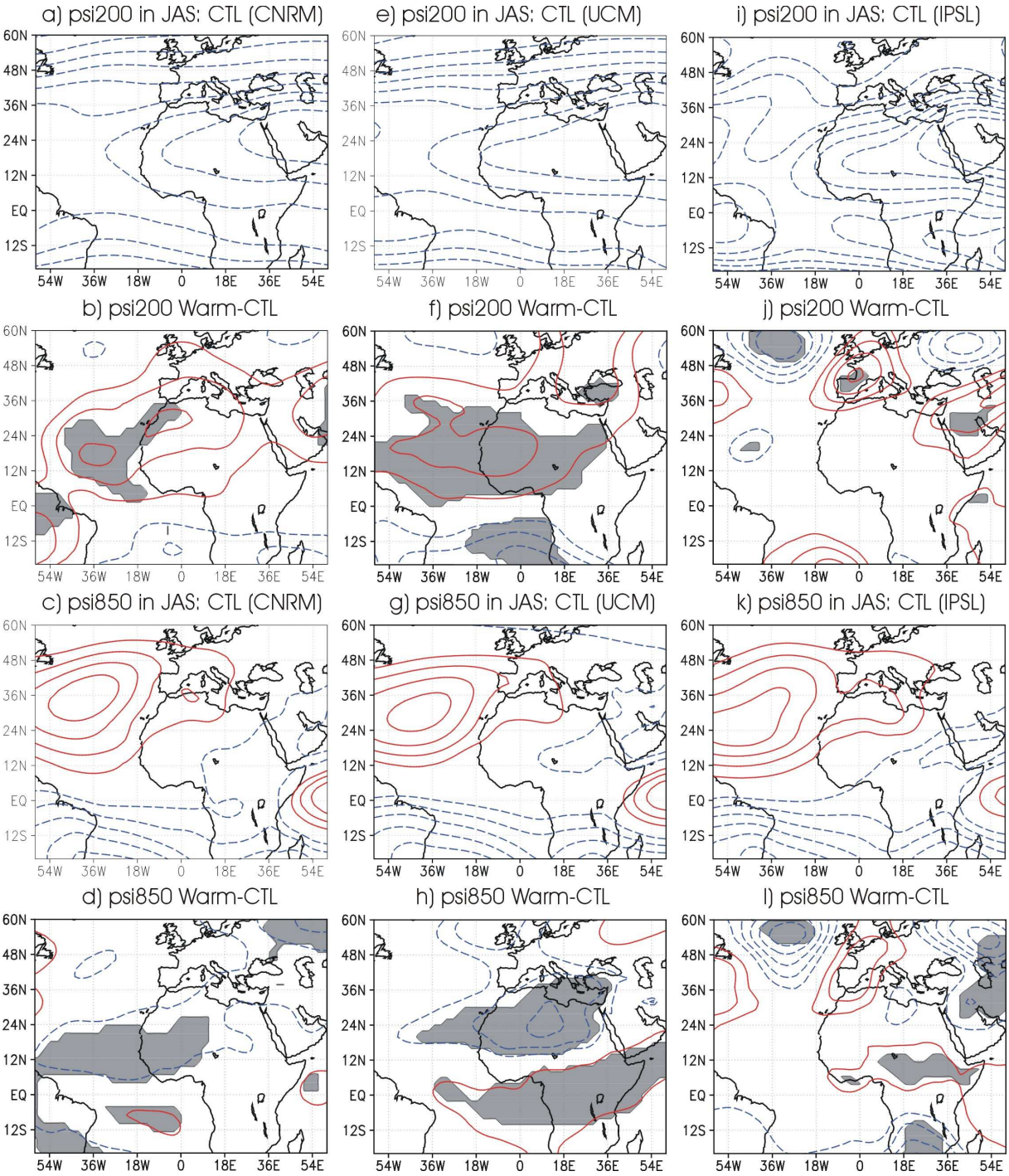

Figure 10: July-September streamfunction composite at 200hPa (first and second rows) and 850hPa (third and fourth rows) from CNRM (**left**), UCM (**middle**) and IPSL (**right**). **First** (ci=1.0 x 10^7 m^2/s) and **Third** (ci=3.0 x 10^6 m^2/s) rows: control runs. **Second** (ci=0.8 x 10^6 m^2/s) and **Fourth** (ci=0.3 x 10^6 m^2/s) rows: warm experiments. Here the shadings refer to significant differences regarding a Student t-test at p=0.05.

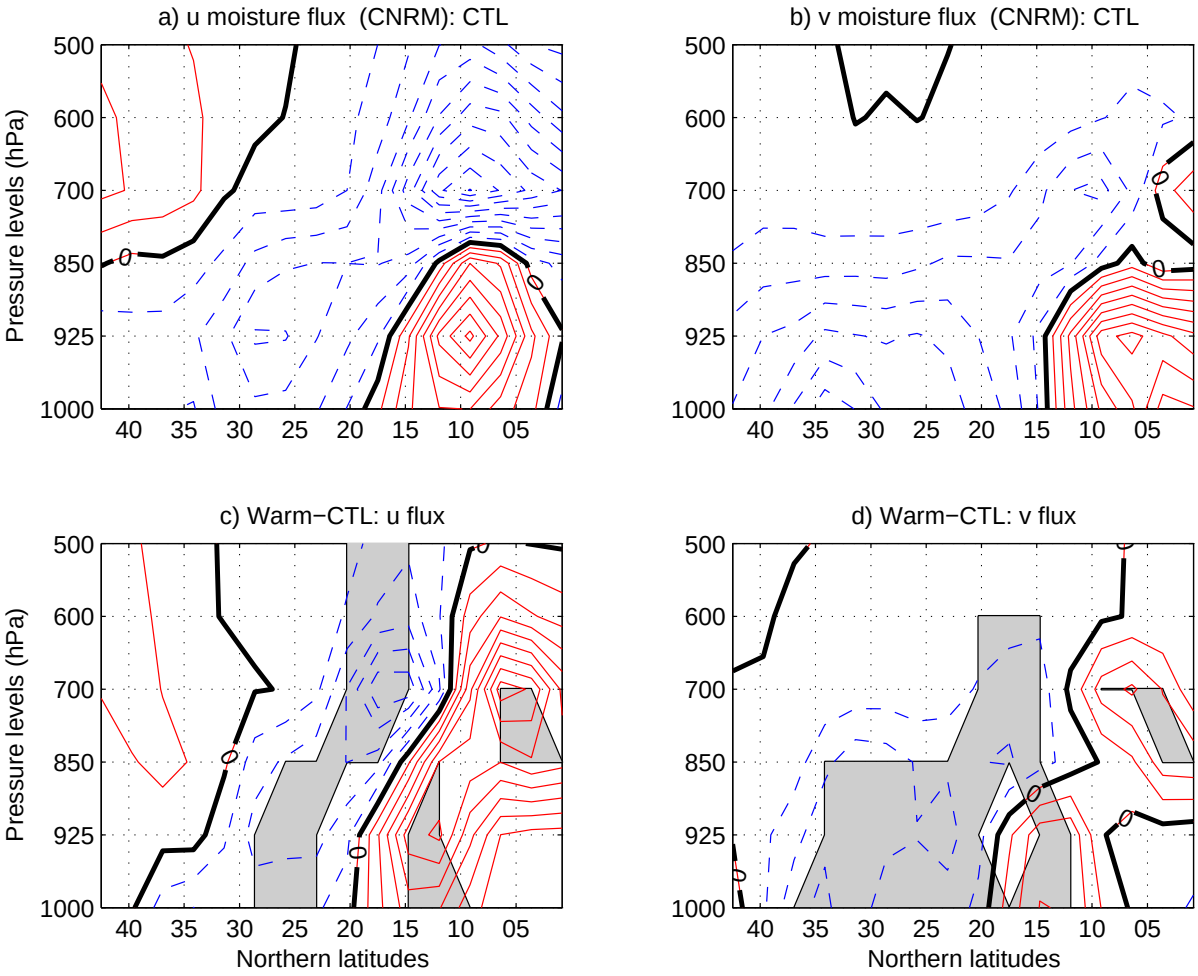

Figure 11: July-September vertical-meridional cross sections of mean and composite moisture fluxes from CNRM over the longitudinal window 20°W-30°E. (**a,b**): u and v mean components from the control runs; (**c,d**): composite differences between the warm and control simulations. The solid (dashed) contours refer to the positive (negative) differences. In panels **c-d**, shadings are superimposed when composite differences are significant at p=0.10 regarding a Student t-test.

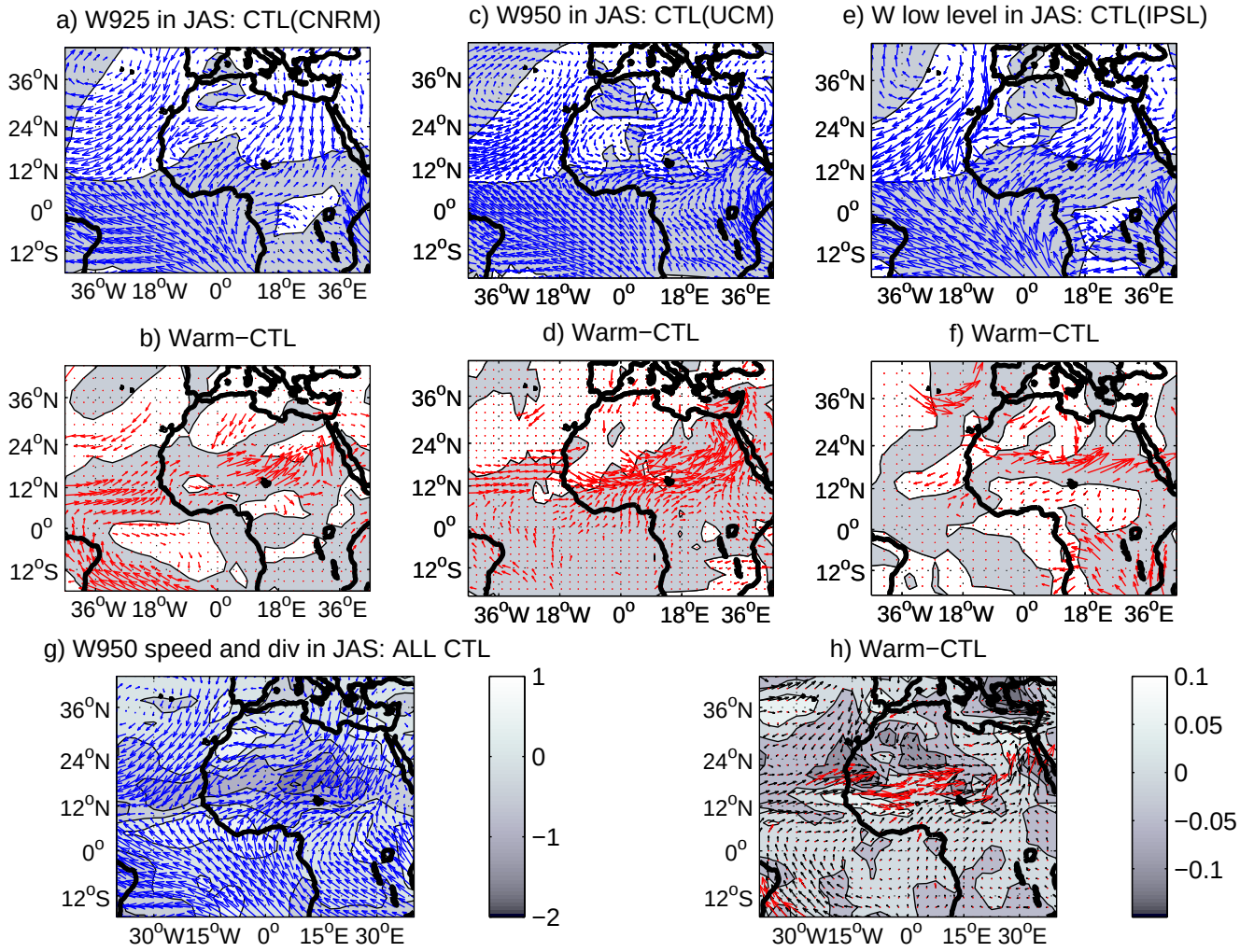

Figure 12: Top: July-September mean wind fields in low levels (925 hPa) from CNRM (**left**)**,** UCM (**middle**) and IPSL (**right**) experiments; control runs with positive meridional wind shaded. **Middle**: Warm minus control differences. Here the shadings refer to significant differences regarding a Student t-test at p=0.10. **Bottom:** Multi-model ensemble of wind (arrows) and horizontal divergence (contours) fields at 950 hPa; mean (**left**) and Warm minus Control composite (**right**). Red arrows are superimposed when the differences on panel h are significant at p=0.10 regarding a Student t-test. Contours refer to the positive (negative) differences in divergence.

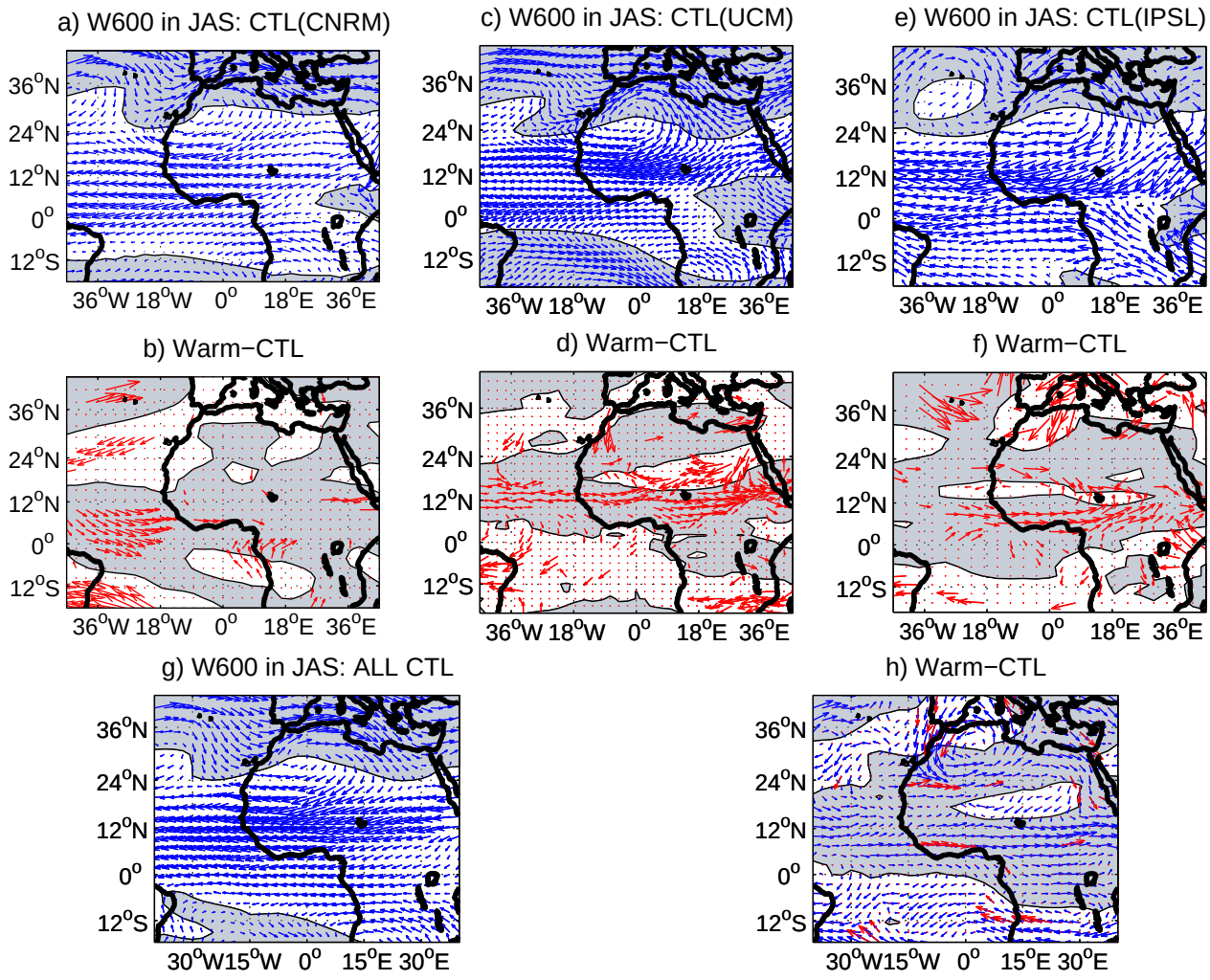

Figure 13: As Fig. 12 but for horizontal flow at 600 hPa. Shading underline positive values.

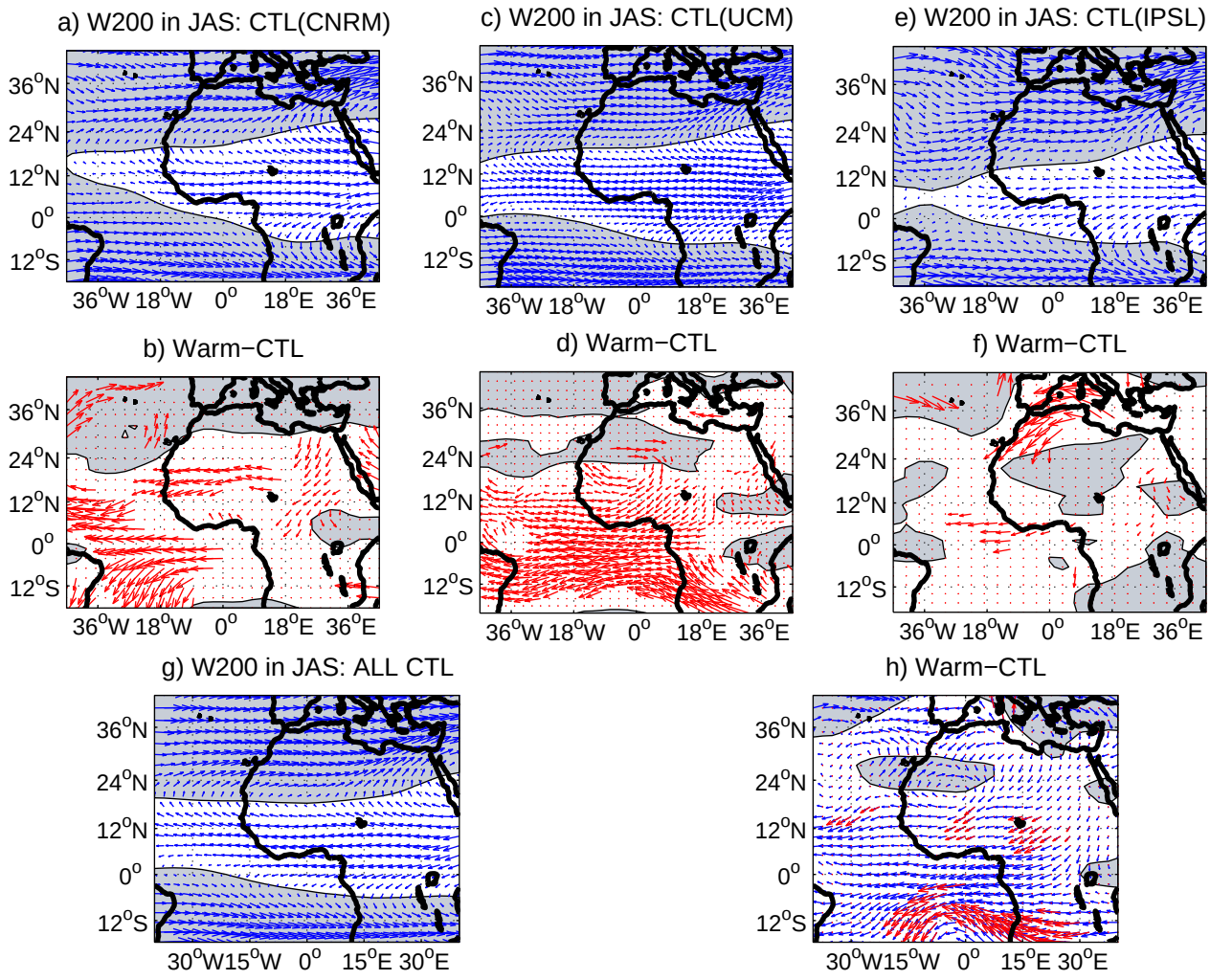

Figure 14: As Fig. 12 but for horizontal flow at 200 hPa. Shadings underline positive values.